DSSS Digital Communications
A SunCam online continuing education course

Direct Sequence Spread Spectrum (DSSS) Digital Communications©

By

Raymond L. Barrett, Jr., PhD, PE
CEO, American Research and Development, LLC

1.0 DSSS Introduction

This course develops the theory and practical issues and examples leading up to Direct Sequence Spread Spectrum (DSSS) Communication. The information theoretic foundation for trading bandwidth and improved Signal-to-Noise Ratio (SNR) is introduced mathematically, but other useful properties associated with particular spreading sequence properties are introduced by example. The gradual development based on the Weaver architecture for frequency translation of single-sideband, suppressed carrier signals through digital QPSK examples into pseudo-noise (PN) sequence spreading of QPSK of sub-carrier sidebands and finally to direct-sequence, spread-spectrum QPSK is employed to build awareness of the relationships between the spectral energy and the modulation processes. The PN sequence generation, its auto-correlation and cross-correlation attributes are introduced and employed in example with a justification for the development of the matched-filter/correlator approach to sequence de-spreading. Some issues of carrier synchronization and problems are introduced but not developed in detail. Finally, the statistical properties of the correlator approach are shown to be the basis for Code-Division, Multiple Access (CDMA) spectrum sharing to ameliorate the extra bandwidth occupied by the spreading.

2.0 Information Theory and Spread Spectrum

In 1948, Claude E. Shannon published his paper "A Mathematical Theory of Communication" containing his famous theorem and tying together prior work by Nyquist and others and starting the study of Information Theory. Today, we express Shannon's theorem in the following equation:

$$C = W \log_2\left(1 + \frac{S}{N}\right) \qquad [2.1]$$

Shannon recognized and proved the relationship between the error-free capacity (***C***) of a channel, its bandwidth (***W***), and the signal-to-noise (***S/N***) ratio of the channel. His work was independent of related work by Nyquist in sampling and discrete-time issues, and Armstrong and the development of wide-band FM radio systems, but helped to augment and explain the performance. We show here a derivation that uses Shannon's theorem to explain the advantages of trading ***W*** and ***S/N*** in spread spectrum and other wideband communication systems. As a first step in explaining the value of wideband and spread spectrum techniques, we express the ratio:

$$\frac{C}{W} = \log_2\left(1 + \frac{S}{N}\right) \qquad [2.2]$$

Amplitude modulation and narrow-band FM systems are concerned with keeping the channel bandwidth narrow and separate from adjacent channels to prevent interference. To a certain extent, some wideband techniques keep the channels separate, too, to avoid and all-or-nothing channel behavior favoring the strongest signal. We shall see that DSSS signal can use the same bandwidth for multiple channels in a more forgiving or sharing fashion. To that extent, DSSS is somewhat "lavish" in the use of bandwidth for reasons that will become apparent. One consequence of DSSS is that the ratio ***C/W*** is usually substantially less than unity with the implication that the ***S/N*** ratio can also be small. Given that we expect ***S/N*** ratio to be small, the number (1+ ***S/N***) is near unity and we would like a way to expand the relationship. We target a well-known series expansion for the natural logarithm as follows:

$$\ln(x) = (x-1) - \frac{1}{2}(x-1)^2 + \frac{1}{3}(x-1)^3 \bullet\bullet\bullet \qquad [2.3]$$

The series expansion for the natural logarithm (base ***e***) has the advantage that it is expanded near unity and rids us of the "pesky" number "1" in the equation, but Shannon expressed his theorem in base 2 arithmetic, so first we convert the base of the logarithm using the relationship:

$$\log_b M = \frac{\log_c M}{\log_c b} \qquad [2.4]$$

$$\log_2 M = \frac{\ln M}{\ln 2} = \frac{\ln M}{.693} = 1.44 \ln M \qquad [2.5]$$

So we can rewrite equation [2.2} as follows:

$$\frac{C}{W} = 1.44 \ln\left(1 + \frac{S}{N}\right) = \ln(1.44) + \ln\left(1 + \frac{S}{N}\right) \qquad [2.6]$$

$$\frac{C}{W} = 1.44\left[\left(\frac{S}{N}\right) - \frac{1}{2}\left(\frac{S}{N}\right)^2 + \frac{1}{3}\left(\frac{S}{N}\right)^3 + \bullet\bullet\bullet\right] \qquad [2.7]$$

Again, given that we expect ***S/N*** ratio to be small:

$$\frac{C}{W} \approx 1.44\left(\frac{S}{N}\right) \qquad [2.8]$$

We see from equation [2.8] that we predict that there exists a spreading ratio ***C/W*** that allows us to support a channel capacity ***C*** with the noise ***N*** far in excess of the signal ***S***. Unfortunately, Shannon states an existence with his proof, but does not include a theory of how to achieve the predicted result. We shall see that coherent correlation in the spreading and de-spreading mechanisms permit just such operation. Further, the coherent de-spreading acts to further spread and lower the effects of non-coherent interfering signals that use the same bandwidth ***W***. We will choose to translate our sources of digital data from its binary representation to DSSS while spreading the signal and retrieve it by dispreading.

3.0 Weaver Modulator: Single Sideband Suppressed Carrier Communication

Signals developed in one part of the spectrum can be translated to another using several means. We choose the "Weaver" architecture for a translation example because it can be implemented easily, comparisons are facilitated, and we can modify it incrementally to make pedagogical points.

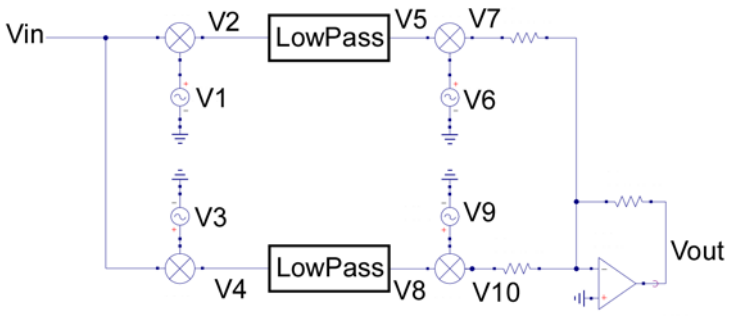

Figure 3.0 "Weaver" Modulator Architecture

The salient features of the original Weaver modulator architecture are the use of four waveform sources, four multiplier or mixer structures, two lowpass filters, and a signal combining adder resulting in a translation of signals from one region of spectrum to another. The waveform sources denoted as V_1 and V_3 form a quadrature pair at the same reference frequency, but with a 90^o phase difference. The waveform sources denoted as V_6 and V_9 form another quadrature pair at the same reference frequency, not necessarily the same frequency as for V_1 and V_3 but also with a 90^o phase difference. ***I*** & ***Q*** channel symbols designate the In-Phase and Quadrature signal paths. The lowpass filters are often designated in the same fashion for reasons that will become apparent.

We develop the architecture from the analog technique to enjoy the relative simplicity of the trigonometric relationships and use that reference as the "gold standard" for spectral

comparison. No spreading is employed and the bandwidth of the Vin signal is translated to another part of the spectrum intact (or spectrally inverted, as we shall see).

Signals developed from the multiplication of two sinusoids may be expressed algebraically using some combination of the following equations. For each trigonometric identity below, the angular terms result in an angular sum and a difference. We choose the α argument to be $\omega_0 t$ and the β argument to be $\omega_1 t$ so that the equations may be expressed as functions of time with those frequencies as follows:

$$\sin\alpha\sin\beta = \frac{1}{2}\cos(\alpha-\beta) - \frac{1}{2}\cos(\alpha+\beta) = \frac{1}{2}\cos(\varpi_0-\varpi_1)t - \frac{1}{2}\cos(\varpi_0+\varpi_1)t \quad [3.0]$$

$$\cos\alpha\cos\beta = \frac{1}{2}\cos(\alpha-\beta) + \frac{1}{2}\cos(\alpha+\beta) = \frac{1}{2}\cos(\varpi_0-\varpi_1)t + \frac{1}{2}\cos(\varpi_0+\varpi_1)t \quad [3.1]$$

$$\sin\alpha\cos\beta = \frac{1}{2}\sin(\alpha-\beta) + \frac{1}{2}\sin(\alpha+\beta) = \frac{1}{2}\sin(\varpi_0-\varpi_1)t + \frac{1}{2}\sin(\varpi_0+\varpi_1)t \quad [3.2]$$

Note that neither the original α, nor β angle survives, nor the original frequencies, only the sum and difference. The suppression of the original frequency components is called "Suppressed Carrier" modulation. We choose the following definitions for the V_{in} signal, V_1 source and V_3 source as follows:

$$V_{in} = A\cos\varpi_0 t \quad [3.3]$$

$$V_1 = B\cos\varpi_1 t \quad [3.4]$$

$$V_3 = B\sin\varpi_1 t \quad [3.5]$$

We can express the V_2 and V_4 products as:

$$V_2 = A\cos\varpi_0 t \bullet B\cos\varpi_1 t = \frac{AB}{2}\cos(\varpi_0-\varpi_1)t + \frac{AB}{2}\cos(\varpi_0+\varpi_1)t \quad [3.6]$$

$$V_4 = A\cos\varpi_0 t \bullet B\sin\varpi_1 t = \frac{AB}{2}\sin(\varpi_0-\varpi_1)t + \frac{AB}{2}\sin(\varpi_0+\varpi_1)t \quad [3.7]$$

We position the lowpass filter characteristic frequency so that the difference frequency passes and the sum frequency is rejected with the result that we produce V_5 and V_8 signals:

$$V_5 = \frac{AB}{2}\cos(\varpi_0 - \varpi_1)t \quad [3.8]$$

$$V_8 = \frac{AB}{2}\sin(\varpi_0 - \varpi_1)t \quad [3.9]$$

We choose the following definitions for the V_6 source and V_9 source:

$$V_6 = C\cos\varpi_2 t \quad [3.10]$$

$$V_9 = C\sin\varpi_2 t \quad [3.11]$$

We can express the V_7 and V_{10} products as:

$$V_7 = \frac{AB}{2}\cos(\varpi_0 - \varpi_1)t \bullet C\cos\varpi_2 t = \frac{ABC}{4}\cos(\varpi_0 - \varpi_1 - \varpi_2)t + \frac{ABC}{4}\cos(\varpi_0 - \varpi_1 + \varpi_2)t \quad [3.12]$$

$$V_{10} = \frac{AB}{2}\sin(\varpi_0 - \varpi_1)t \bullet C\sin\varpi_2 t = \frac{ABC}{4}\cos(\varpi_0 - \varpi_1 - \varpi_2)t - \frac{ABC}{4}\cos(\varpi_0 - \varpi_1 + \varpi_2)t \quad [3.13]$$

We can express the V_{out} sum as:

$$V_{out} = V_7 + V_{10} = \frac{ABC}{2}\cos(\varpi_0 - \varpi_1 - \varpi_2)t \quad [3.14]$$

The system performance for the Weaver architecture is met by this realization and a few qualitative points can be made. There are no constraints on the locations of the three frequencies, other that the need to pass the first difference and reject its sum using the lowpass filter. The primary function of the two "channels" in the architecture is to develop the quadrature relationship between the lowpass filter output signals. The lowpass filters each must pass the difference signal, including any DC components, so they are often referred to as "baseband" filtering. The arithmetic differences are "two-sided" and can be thought of as a symmetrical difference around the ω_1 frequency. If an equivalent band-limited signal with the same spectral content is available, only the final stages are required.

4.0 Low Frequency Analog Weaver Modulator: An Example

As illustrated in Figure 4.0 below, we construct the V_{in} signal with a V_0 center frequency at 1500 Hertz. We construct the Weaver modulator with two quadrature sine-wave pairs with the V_1 and V_3 pair in quadrature at 1000 Hz, and the V_6 and V_9 pair in quadrature at 2200 Hz. We have chosen relatively unrelated frequencies to make the spectral content easy to

identify. We have chosen relatively low frequencies so that the illustrations can contain all pertinent waveforms near each other in time and frequency.

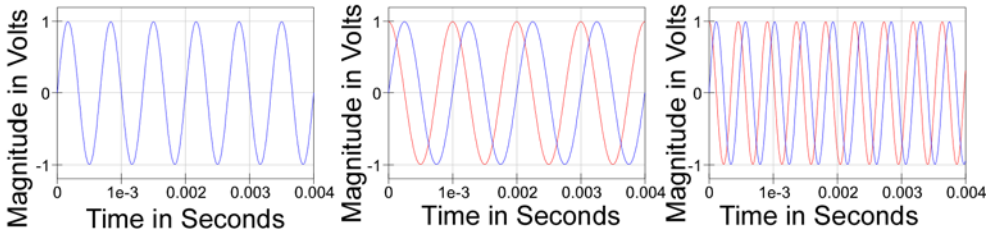

Figure 4.0 V_0 at 1500 Hz, V_1 & V_3 at 1000 Hz, and V_6 & V_9 at 2200 Hz

We choose to produce the V_{in} for the example as a tone burst so that the spectral characteristics are similar to the original Weaver usage for speech signals. It is a naïve approximation, but makes clear identification of time and frequency effects a bit easier.

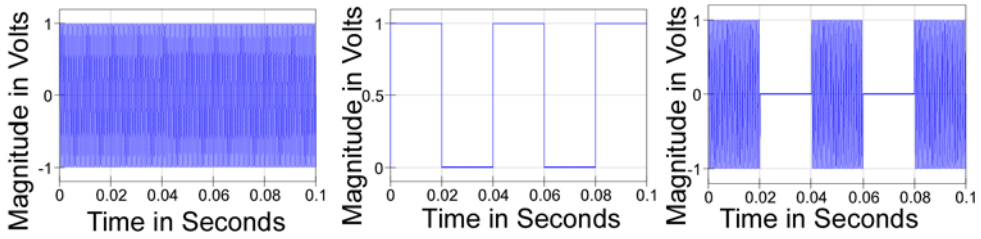

Figure 4.1 V_0 at 1500 Hz, 25 Hz Square Modulation, and V_{in} Tone Burst

As illustrated in figure 4.1 above, we construct the V_{in} signal with a V_0 center frequency at 1500 Hertz by modulating the 1500 Hz sine wave with a square-wave at 25 Hz to produce the V_{in} tone burst. The square-wave tone burst for the V_{in} is clearly distinct from the sine-wave sources inside the Weaver modulator.

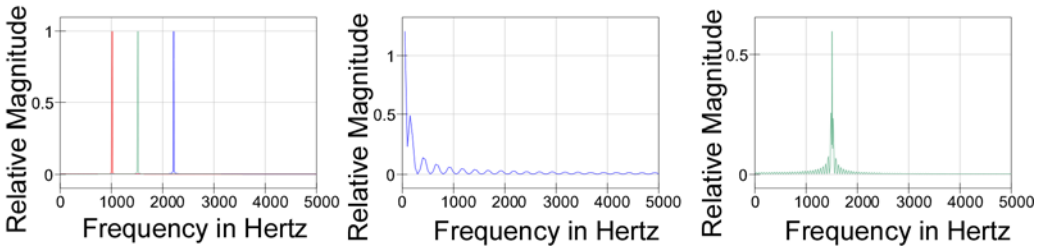

Figure 4.2 V_0, V_3 & V_9 Spectra. 25 Hz Modulation Spectrum, and V_{in} Spectrum

As illustrated in Figure 4.2 above, we see that each sine wave source results in single spectral line at a single frequency, but the square waveform of the modulation has the expected odd-harmonic spectrum of the 25 Hz frequency due to its shape, and that shape produces the side-bands around the carrier in the V_{in} spectrum.

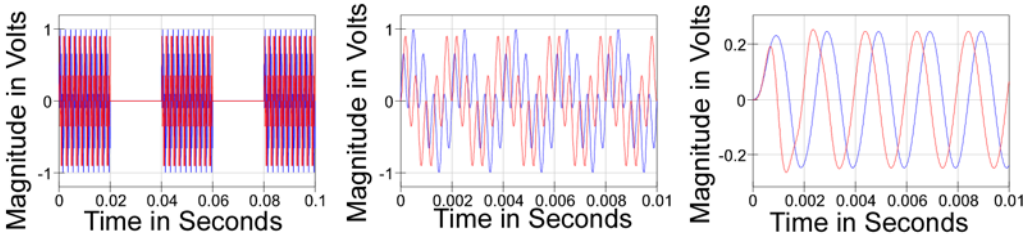

Figure 4.3 V_2 & V_4 Bursts. V_2 & V_4 Burst Detail, and V_5 & V_8 Burst Detail

As illustrated in the time domain in Figure 4.3 above, we see that the multiplication of the tone-burst modulated V_{in} signal located around 1500 Hz by the V_1 and V_3 pair in quadrature at 1000 Hz, produces similarly shape tone bursts at the corresponding V_2 and V_4 signal locations. As we expect from equations [12.6] and [12.7], the result contains the difference at 500 Hz, and the sum at 2500 Hz, as the detail confirms. Following the lowpass filters, however, the V_5 and V_8 signal locations present only the 500 Hz difference frequency components, and more important, those differences are in quadrature to each other.

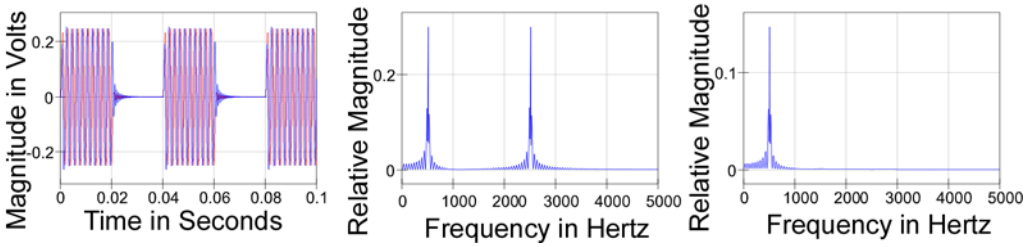

Figure 4.4 V_5 & V_8 Burst. V_2 & V_4 Spectra Detail, and V_5 & V_8 Spectra Detail

As illustrated in the spectra in Figure 4.4 above, we see that the multiplication of the tone-burst modulated V_{in} signal located around 1500 Hz by the V_1 and V_3 pair in quadrature at 1000 Hz, produces the V_2 and V_4 spectra that contain the difference at 500 Hz, and the sum at 2500 Hz, as the detail reveals. Following the lowpass filters, however, the V_5 and V_8 signal locations present only the 500 Hz difference frequency spectra. The spectra do not reveal the quadrature relationship as found in the time domain traces, but indicate tone burst sidebands.

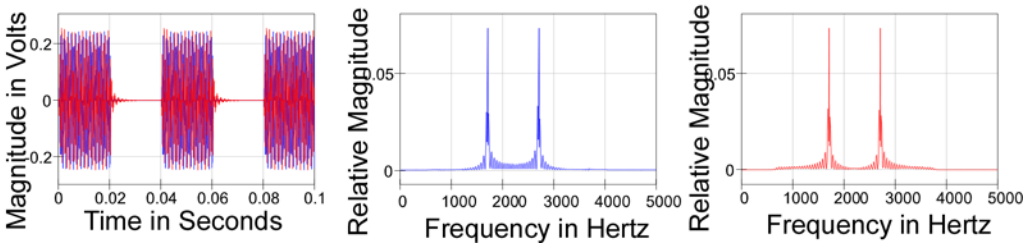

Figure 4.5 V_7 & V_{10} Carrier Bursts. V_7 Spectra Detail, and V_{10} Spectra Detail

Figure 4.5 above shows that the multiplication of the 500 Hz frequency tone-burst modulated V_5 and V_8 signals by the V_6 and V_9 carrier pair in quadrature at 2200 Hz, produces the V_7 and V_{10} signals with spectra that contain the difference at 1700 Hz, and the V_{out} sum at 2700 Hz, as the detail reveals, and we expect from the results of the trigonometric identities, but the carrier itself is suppressed

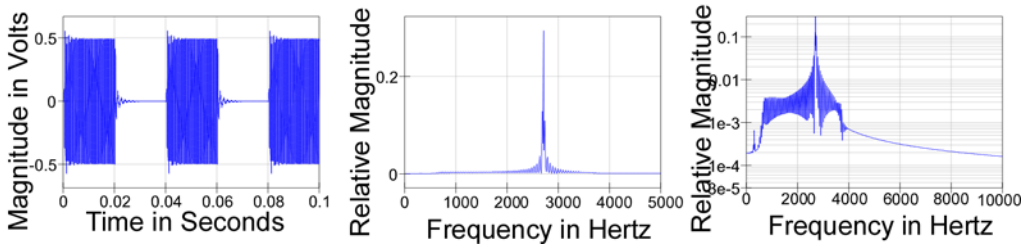

Figure 4.6 V_{out} Burst. V_{out} Spectra, and V_{out} Spectra Logarithmic

Finally, we see the confirmation in figure 4.6 that shows that the Weaver modulator has translated a tone burst signal centered 500 Hz above the V_1 and V_3 quadrature pair at 1000 Hz, to preserve the tone burst modulation to be centered at 2700 Hz, or 500 Hz above the V_6 and V_9 quadrature pair frequency at 2200 Hz.

The Weaver Modulator could be used as easily to translate a 5 kHz wide speech channel from near baseband up to the GHz range, but the illustrations would be more difficult for the purposes of this course.

5.0 Phase Modulated Weaver Modulator: Upper and Lower Sidebands

We show the effect of inverting either, or both of the V_5 and V_8 signal magnitudes and the effect on the output signal to demonstrate the existence of upper and lower translation sidebands.

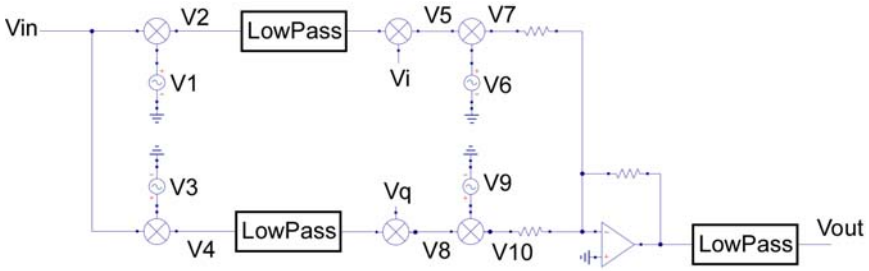

Figure 5.0 Weaver Architecture with V_i and V_q Phase Modulation

In figure 5.0 above, we insert multipliers that are constrained to have a static plus or minus 1 magnitude showing the effects on the $\boldsymbol{V_{out}}$ signal, in particular on upper and lower sidebands. With both signals at +1 value, we have all the prior results.

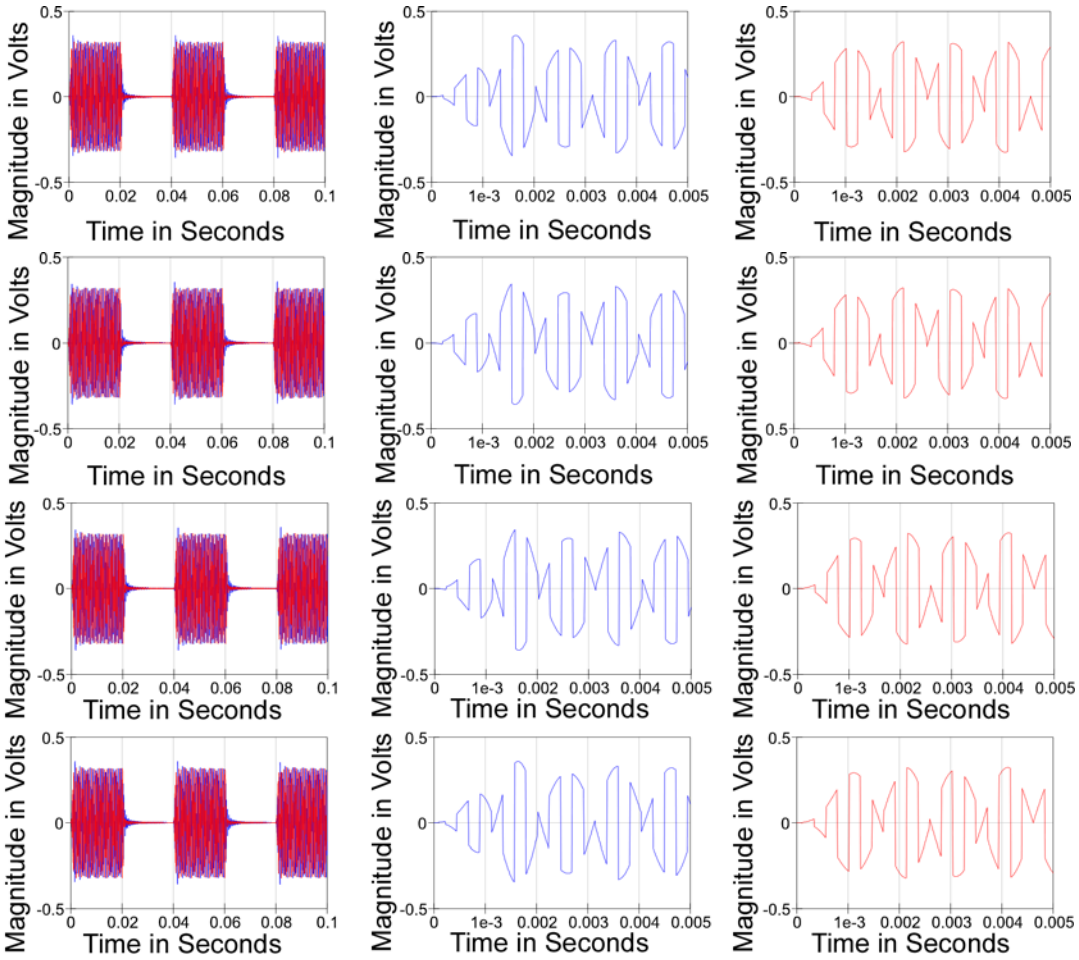

Figure 5.1 V_7 & V_{10} Burst Waveform, V_{10} Burst Detail, and V_7 Burst Detail

In figure 5.1 above, we compare the four cases of the V_7 and V_{10} Burst Waveforms with both V_i and V_q = +1, then V_i = -1 and V_q = +1, then both V_i and V_q = -1, and finally V_i = +1 and V_q = -1, with the noticeable effect of the phase reversals in the burst details.

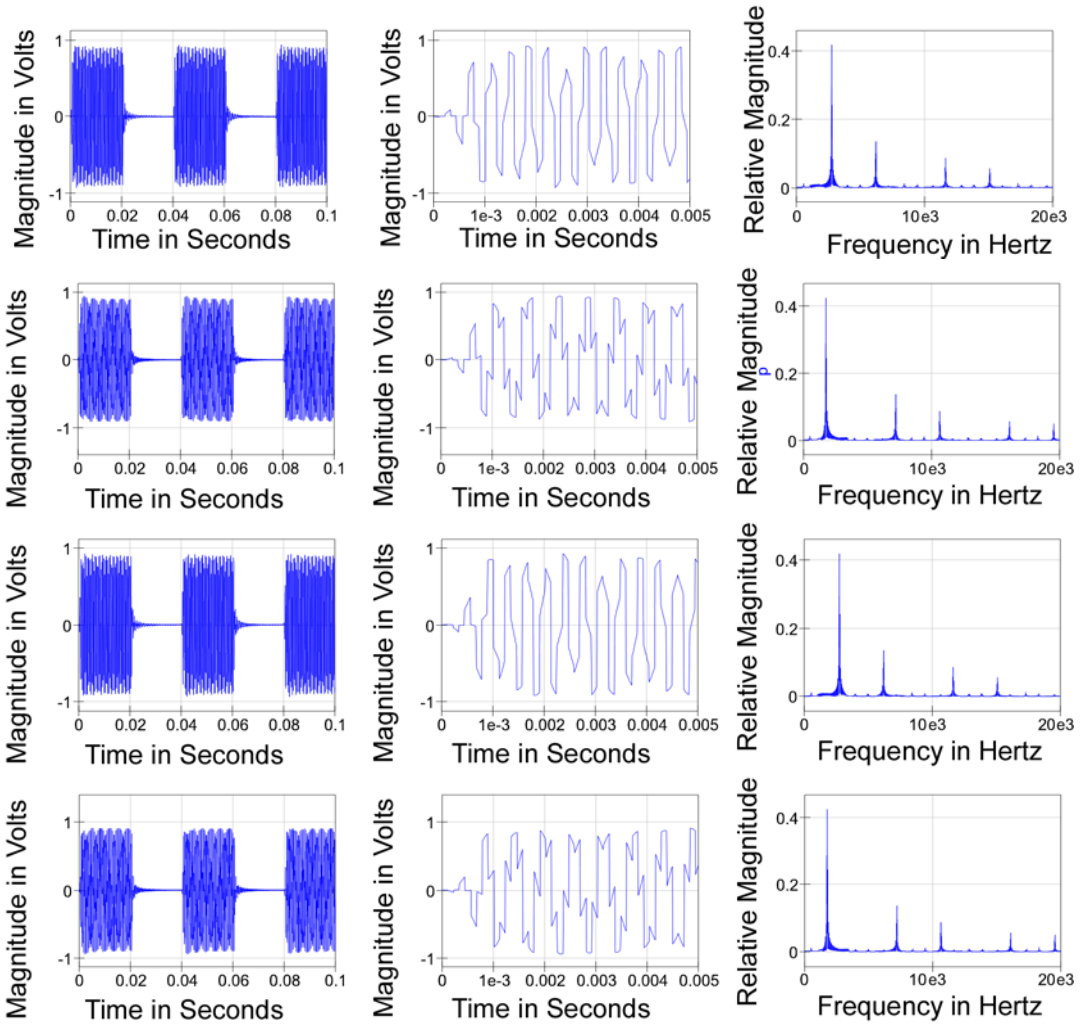

Figure 5.2 V_{out} Burst. V_{out} Burst Detail, and V_{out} Spectra

In figure 5.2 above, we compare the four cases of the $\boldsymbol{V_{out}}$ Burst Waveforms, their detail, and spectra with both V_i and V_q = +1, then V_i = -1 and V_q = +1, then both V_i and V_q = -1, and finally V_i = +1 and V_q = -1, with the noticeable $\boldsymbol{V_{out}}$ wave-shape effect of the phase reversals in the burst details, and the change of spectra. We originally constructed the Weaver modulator so that summation at the output would cancel a difference in frequencies and add

the sum of frequencies terms. Each time we alter one phase of the V_7 and V_{10} waveforms, the $\boldsymbol{V_{out}}$ wave-shape is change so that the cancellation changes between sum of frequencies and difference of frequencies. We call the sum of frequencies (2200 Hz + 500 Hz = 2700 Hz) the "upper-sideband," and the difference of frequencies (2200 Hz - 500 Hz = 1700 Hz) the "lower-sideband," relative to the V_6 and V_9 quadrature pair frequency at 2200 Hz.

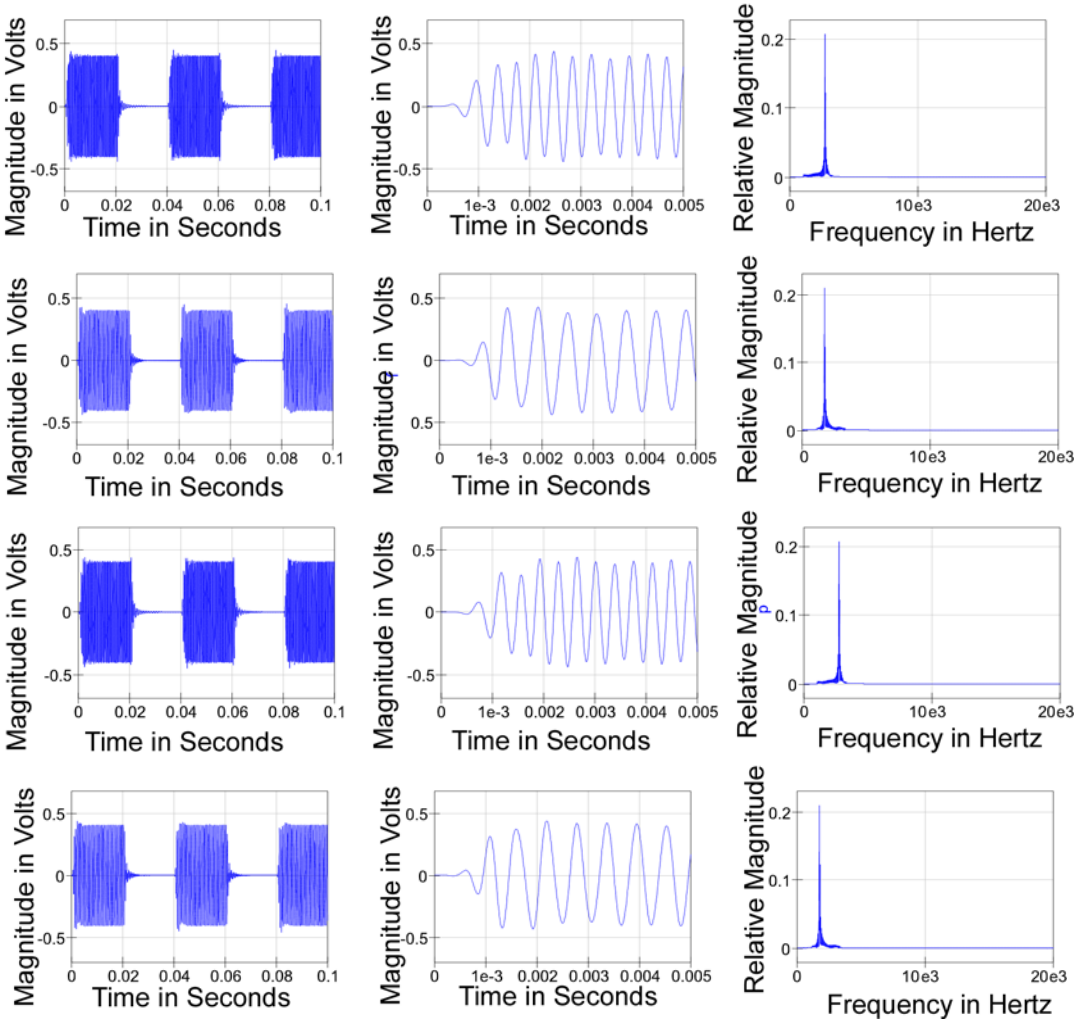

Figure 5.3 Filtered V_{out} Burst. Filtered V_{out} Burst Detail, and Filtered V_{out} Spectra

In figure 5.3 above, we compare the four cases of the $\boldsymbol{V_{out}}$ Burst Waveforms as they appear after filtering by the harmonic suppression lowpass filter, their detail, and spectra with both V_i and V_q = +1, then V_i = -1 and V_q = +1, then both V_i and V_q = -1, and finally V_i = +1 and V_q = -1, with the noticeable $\boldsymbol{V_{out}}$ frequency and phase-reversals. The phase reversals in the burst

details reveal that the upper sideband combinations have180^{o} difference between them, as do the lower sideband instances. The change of spectra shows only the frequencies related to the upper or lower sideband productions, but no information about the phase. We originally constructed the Weaver modulator so that summation at the output would cancel a difference in frequencies and add the sum of frequencies terms.

6.0 Modified Weaver Modulator: QPSK

We show in figure 6.0 below a modified form of the Weaver modulator that retains the phase modulation multipliers use explored in the section above, but eliminates the V_{in} connection for the voice signal, the tone burst, the filters, and the first multiplier set. Instead, we have supplied the quadrature pair of sources ***V5ki***, and ***V5kq*** that are the equivalent to the stages we have removed for a steady-state case with no equivalent V_{in} tone burst modulation. Here we intend to explore the four cases of phase modulation that we introduced in the section above. We have also scaled the input frequency 10x up to 5 kHertz and the carrier frequency 10x up to 22 kHertz in anticipation of significant spreading in later discussions.

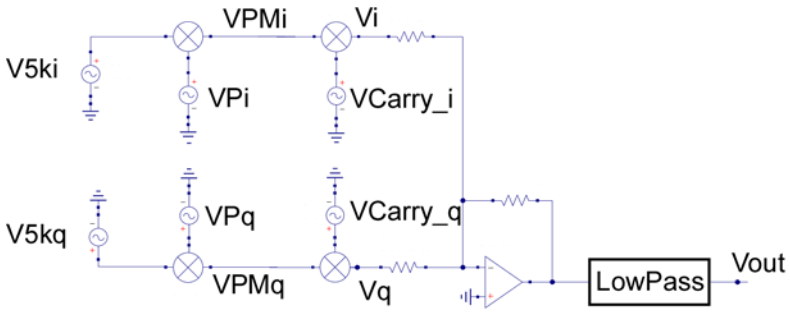

Figure 6.0 Weaver Modulator for Quadri-Phase-Shift Keying QPSK

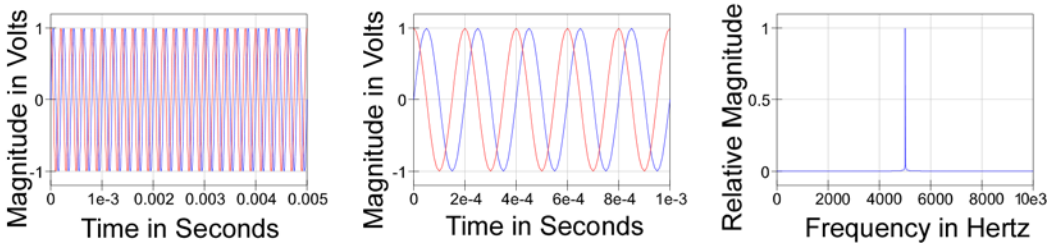

Figure 6.1 V5ki and V5kq Un-Modulated 5 kHertz Quadrature Sine Wave Sources

We saw that there are four distinct cases for the phases of the ***VPMi*** and ***VPMq*** signals that we previously designated in the prior section as V_5 and V_8 signals. Here we use the a new

designation because we stress the phase modulation of the signals. We saw that 180^{o} phase shifts occurred in each signal and resulted in the V_{out} producing either the upper sideband or lower sideband depending on the particular combination. We indicate below a "Constellation" of the four possible phase combinations corresponding the ***VPi*** and ***VPq*** polarities.

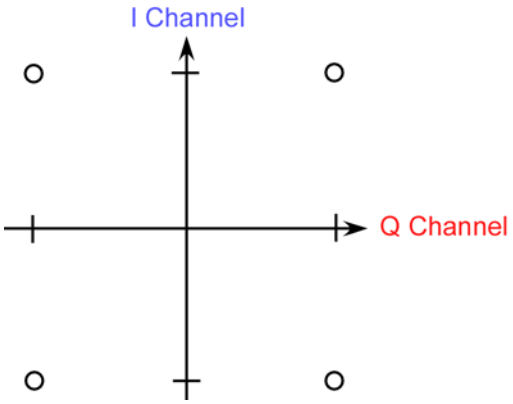

Figure 6.2 Weaver Modulator QPSK "Constellation"

We saw that signals in the first and third quadrants corresponding to the phase modulation being presented with matching polarity produced only the upper sideband, while mismatched polarities produced only the lower sideband. The constellation in figure 6.2 represents the four cases with the polarities indicated as positive in the direction of the arrows.

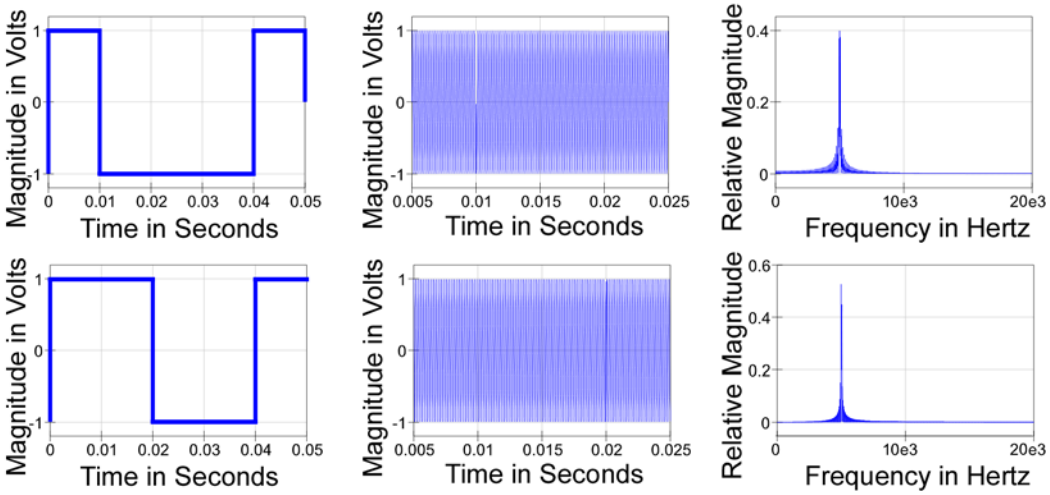

Figure 6.3 *VPi* (top) and *VPq* (bottom), *VPMi* (top) and *VPMq* (bottom), and Spectra

In figure 6.3 above, we introduce a dynamic +/- pattern to the ***VPi*** (top) and ***VPq*** (bottom) phase modulating multiplier inputs. The multipliers produce the ***VPMi*** (top) and ***VPMq*** (bottom) phase-modulated signals and their resulting spectra. Each pattern makes its transition edges with a 10 msec periodicity, as if a 100 Hertz bit-rate clock produced the pattern. Therefore, we can infer that the ***VPi*** (top) pattern represents a binary 10001 sequence and the ***VPq*** (bottom) pattern represents a binary 11001 sequence. Because each pattern has a run-length of five bits, there is non-zero DC content to each pattern and there is some small DC component in each, producing significant energy at the 5 kHertz modulation frequency in the spectrum. Because pattern produces 0^o and 180^o phase states between changes, ***VPMi*** (top) and ***VPMq*** (bottom) are two 5 kHertz "BiPhase" modulated signals with each 5 kHertz carrier in quadrature. It is these biphase modulation effects that produce the spectra centered on 5 kHertz. The DC component of the data prevents the 5 kHertz from being a suppressed carrier as in the prior examples.

In figure 6.3 above, in the ***VPMi*** (top) and ***VPMq*** (bottom) spectra, there are no harmonics of the 5 kHertz produced because the ***V5ki***, and ***V5kq*** source signals that we have bi-phase modulated were sine wave sources and had no harmonics themselves. The ***VPi*** (top) and ***VPq*** (bottom) phase modulating multiplier input patterns are digital data and have significant energy at multiples of their equivalent 100 Hertz bit-rate clock that appear as sidebands in the ***VPMi*** (top) and ***VPMq*** (bottom) spectra.

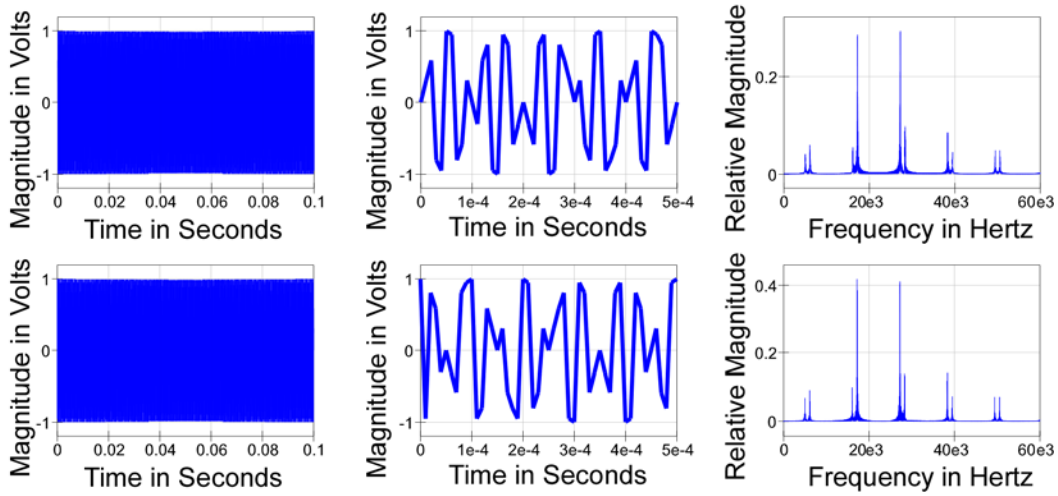

Figure 6.4 *Vi* (top) and *Vq* (bottom), *Vi* (top) and *Vq* (bottom) Detail, and Spectra

In figure 6.4 above, in the ***Vi*** (top) and ***Vq*** (bottom) signals, we see the constant envelope, phase modulation signals, but in the detail the square wave nature of the ***VCarry_i*** (used in the top) and ***VCarry_q*** (used for the bottom) signals used as the carrier quadrature pair are evident because the phase changes from the multiplication are abrupt. The ***Vi*** (top) and ***Vq*** (bottom) spectra produced have the harmonic multiples of the 22 kHertz carrier square waves, along with the modulation spectra around them. There is no DC component evident in the spectra, and because the ***VPMi*** and ***VPMq*** signals had no DC component, the spectra of the ***Vi*** (top) and ***Vq*** (bottom) are suppressed carrier with no content at the 22 kHertz carrier frequency itself, only its upper and lower sidebands. Note that the ***Vi*** (top) and ***Vq*** (bottom) spectra sidebands are each symmetrical around the suppressed carrier, but each set has a different symmetrical magnitude. Notice they are also 5 kHertz from the carrier now.

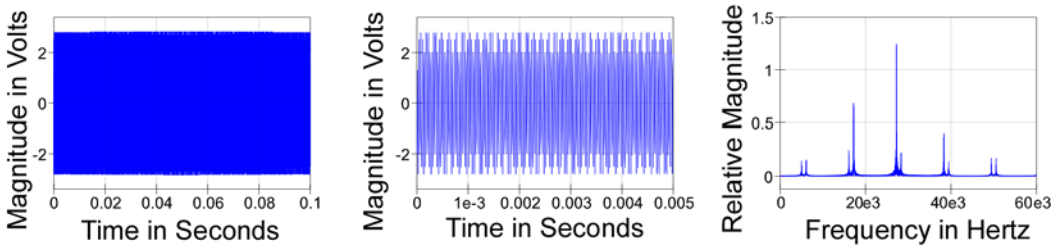

Figure 6.5 Un-Filtered Sum of *Vi* and *Vq* Signals Detail, and Spectrum

In figure 6.5 above, we show the un-filtered sum of the ***Vi*** and ***Vq*** suppressed carrier signals. The summation produces a double-sideband, suppressed carrier result, but the summation has a produced sideband set with substantial asymmetry in the energy of the sidebands. This data sequence has produced more energy in the upper sideband than in the lower sideband. Also, the un-filtered nature of the summation has retained the harmonic content produced by the use of square wave sources in the production of the ***Vi*** and ***Vq*** suppressed carrier signals.

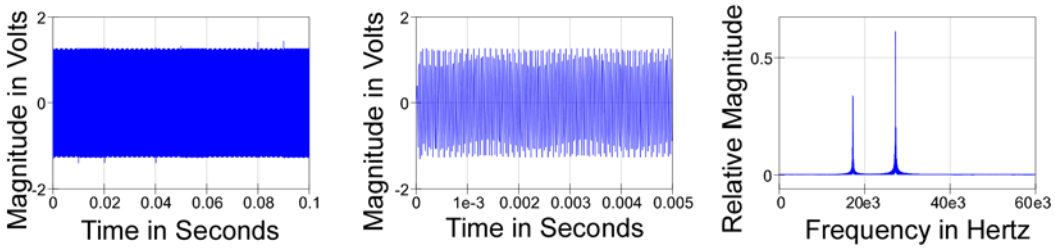

Figure 6.6 *Vout* Low Pass Filtered Sum of *Vi* and *Vq* Signals Detail, and Spectrum

In figure 6.6 above, we show the ***Vout*** filtered sum of the ***Vi*** and ***Vq*** suppressed carrier signals. The detail reveals that the result is a much "smoother" waveform and the spectrum

shows that the harmonics have been suppressed. The filtered sum also shows the same relative ratio of sideband signal energy is retained around the original carrier frequency at 22 kHertz. ***Vout*** is a double-sideband, suppressed-carrier signal with no DC component and suitable for a "channel" of communications.

In figure 6.7 below, we will employ a replica of the original Weaver modulator with different parameters to recover some of the information contained in this ***Vout*** signal.

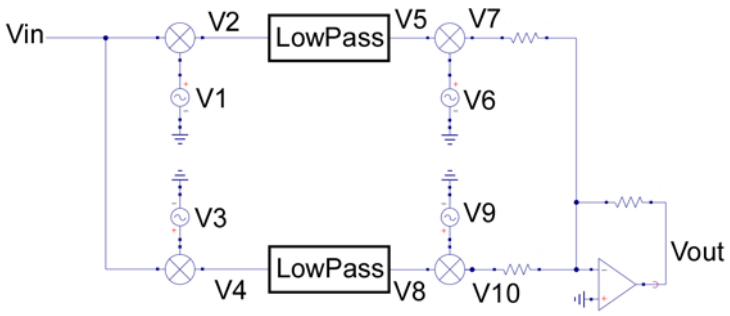

Figure 6.7 Weaver Modulator Used for Demodulation Discussion

In figure 6.7 above, we show the Weaver structure used for demodulation of the ***Vout*** signal shown in figure 6.6 further above. Later we will develop other demodulation structures and this one is used only in this local context for discussion of demodulation issues. At the location of the quadrature source pair ***V1*** and ***V3*** in figure 6.7 above, we employ a replica of the ***VCarry_i*** and ***VCarry_q*** square wave quadrature signal pair for demodulation and connect the ***Vin*** input terminal to the filtered ***Vout*** signal shown in figure 6.6 further above.

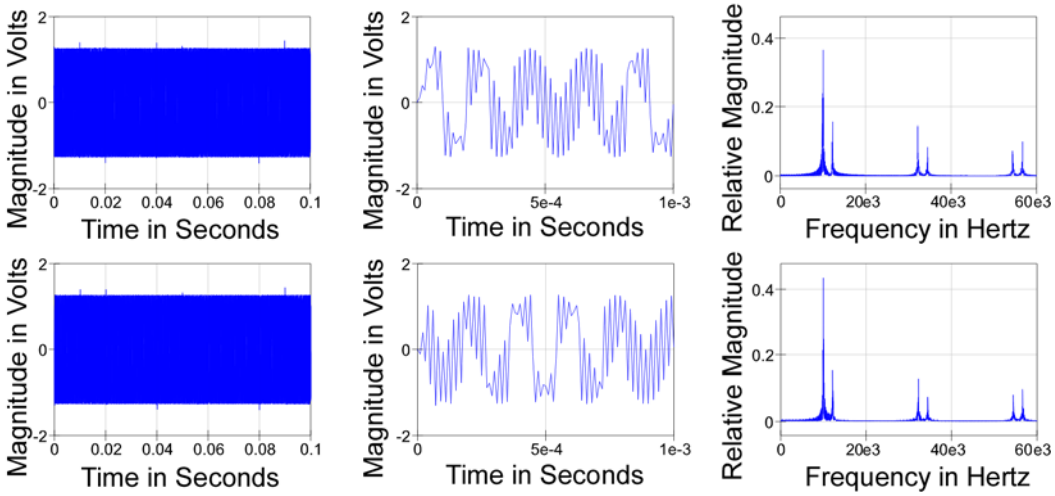

Figure 6.8 *V2* (top) and *V4* (bottom), *V2* (top) and *V4* (bottom) Detail, and Spectra

In figure 6.8 above, we show the waveforms of the ***V2*** (top) and ***V3*** (bottom) signals developed in the de-modulator of figure 6.7 above. We see a constant envelope, phase modulation signals, but in the detail we see remnants of the square wave nature of the ***V1*** (used in the top) and ***V3*** (used for the bottom) signals used as the carrier quadrature demodulation pair because the detail phase changes from the multiplication are abrupt. The ***V2*** (top) and ***V4*** (bottom) spectra produced have the harmonic multiples of the 22 kHertz carrier square waves, along with the modulation spectra around them, and now show the difference frequency components produced at the 5 kHertz demodulation frequency.

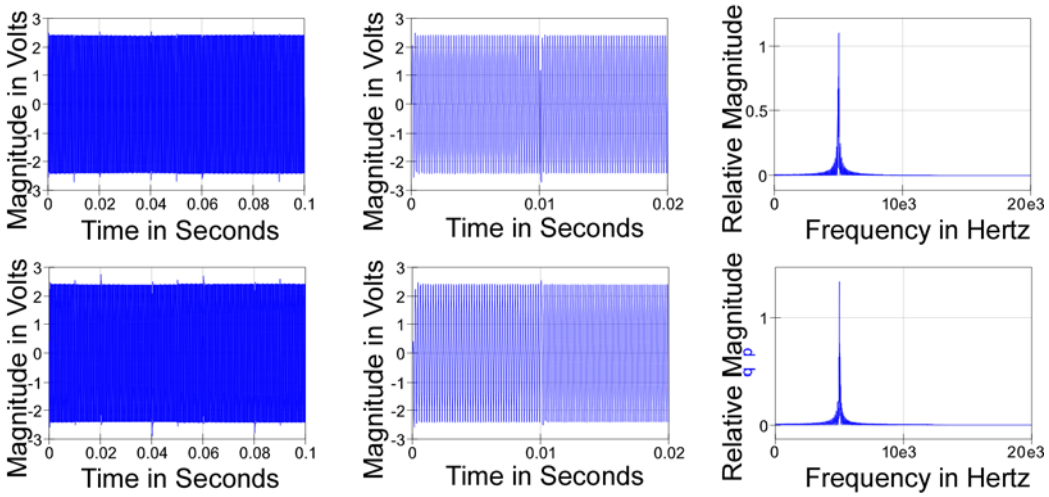

Figure 6.9 *V5* (top) and *V8* (bottom), *V5* (top) and *V8* (bottom) Detail, and Spectra

Filtering the ***V2*** (top) and ***V4*** (bottom) signals leaves the ***V5*** (top) and ***V8*** (bottom) filtered signals that replicate the ***VPMi*** and ***VPMq*** phase-modulated signals produced in the prior figure 6.3 of the transmitting Weaver modulator. These signals are QPSK replicas, but there are well-known issues of identifying which replica channel represents which transmitter channel, as well as the exact frequency/phase synchronization of the ***V1*** and ***V3*** signals with the ***VCarry_i*** and ***VCarry_q*** square wave quadrature signal pair used in the transmitter. We defer that discussion until after we have introduced the pseudo-noise spreading of the QPSK transmitted signal and discussed its synchronization in a receiver.

7.0 Pseudo-Noise (PN): Independent DSSS I & Q Spectrum Spreading

Before we introduced the structures and discussion of QPSK and the Weaver modulator, we made remarks about Direct Sequence Spread Spectrum (DSSS) and the implications of

Shannon's theorem in the benefits of wider bandwidths. We now introduce the maximal-length pseudo-random binary sequence (PRBS), refer to it as a Pseudo-Noise (PN) sequence, demonstrate two of the shortest PN sequences, their auto-correlation and cross-correlation behaviors and use as spreading sequences for digital data for QPSK. We introduce two such sequences so that we can employ them as independent operations for the ***I*** and ***Q*** channel information.

We present a digital shift-register structure for generating a maximal-length pseudo-random binary sequence below in figure 7.0, and refer the reader to research the French mathematician E. Galois for detail on finite field arithmetic. For a shift-register of "N' bits length, we have the possibility of representing 2^N possible distinct states. The technique we present permits a structure to visit all but one of these states in a cycle-sequence using very little hardware. The remaining single state, however, must be avoided because it can persist. We see that our technique is synchronous to a clocking signal and the remaining "forbidden" state can be detected and forced to another state in the cycle.

We define a "***D***" Flip/Flop relationship:

$$Q_{n+1} = D_n \qquad [7.0]$$

The next value of the "***Q***" contents is equal to the present contents of the "***D***" input, and contents change synchronously with the clock. We also include an auxiliary "Reset" input "***R***" that asynchronously forces a ***Q*** = 0 condition, regardless of other stimuli.

For both cases to be employed, we use a collection of three "***D***" Flip/Flops and consequently we have $2^N - 1 = 8 - 1 = 7$ possible distinct states. We designate the three "***D***" Flip/Flops using $\boldsymbol{Q_A}$, $\boldsymbol{Q_B}$, and $\boldsymbol{Q_C}$ designators with the inputs corresponding as $\boldsymbol{D_A}$, $\boldsymbol{D_B}$, and $\boldsymbol{D_C}$. We connect the three "***D***" Flip/Flops as a "Shift Register" with:

$$D_B = Q_A \qquad [7.1]$$

$$D_C = Q_B \qquad [7.2]$$

We connect each shift register reset signals in a common connection so that reset condition causes:

$$Q_A = Q_B = Q_C = 0 \qquad [7.3]$$

For each distinct PRBS, we use a distinct generator polynomial according to Galois that consists of a binary "Exclusive NOR" combination of the contents of the shift register to generate the $\boldsymbol{D_A}$ input.

$$D_A = \overline{Q_C \oplus Q_A} \qquad [7.4]$$

$$D_A = \overline{Q_C \oplus Q_B} \qquad [7.5]$$

We present results in tabular form in Table 7.0, as follows:

Table 7.0 PRBS Generation

		$D_A = XNOR(Q_C, Q_A)$				$D_A = XNOR(Q_C, Q_B)$			
N	**R**	**Q_A**	**Q_B**	**Q_C**	**D_A**	**Q_A**	**Q_B**	**Q_C**	**D_A**
0	1	0	0	0	1	0	0	0	1
1	0	1	0	0	0	1	0	0	1
2	0	0	1	0	1	1	1	0	0
3	0	1	0	1	1	0	1	1	1
4	0	1	1	0	0	1	0	1	0
5	0	0	1	1	0	0	1	0	0
6	0	0	0	1	0	0	0	1	0
7	0	0	0	0	1	0	0	0	1

The sequences in Table 7.0 above are distinct and representing the Q_A, Q_B, and Q_C contents as binary numbers, the sequences are: 0, 4, 2, 5, 6, 3, 1 on the left and 0, 4, 6, 3, 5, 2, 1 on the right at the corresponding instants. The table and its sequence contents are left-to-right in the same order as the schematic shift register representations in figure 7.0 below.

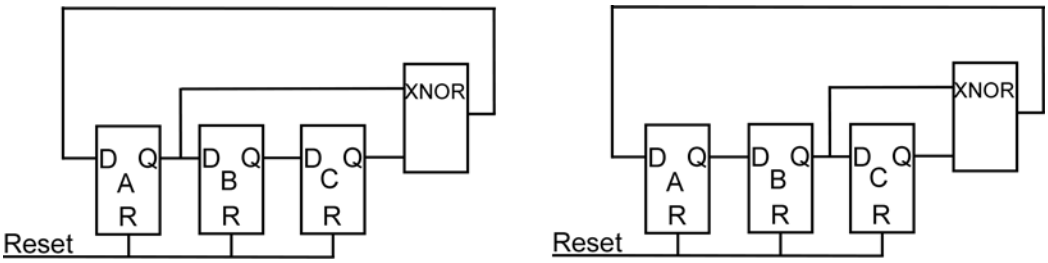

Figure 7.0 The Two Three-Stage Shift-Register Structures for PRBS Example

We have not shown the common clocking, nor the logic needed to detect the persistent binary Q_A, Q_B, and Q_C = 1 or "7" state. In case the state is ever accidentally entered, an "all 1" condition produces a reset that will cause at least one Flip/Flop to reset to "0" before the condition is removed.

We have chosen this particular implementation of the PRBS generator because it illustrates the same sequence in a generator that is available with four different delays. We shall see

later that having the sequence as well as “early” and “late” versions available enhances sequence synchronization.

Table 7.1 PRBS Sequence (Left) Autocorrelation

D_A	1	0	1	1	0	0	0	
Shift								**Matches**
1	0	1	0	1	1	0	0	3
2	0	0	1	0	1	1	0	3
3	0	0	0	1	0	1	1	3
4	1	0	0	0	1	0	1	3
5	1	1	0	0	0	1	0	3
6	0	1	1	0	0	0	1	3
7	1	0	1	1	0	0	0	7

In Table 7.1 above, we show the $\boldsymbol{D_A}$ input sequence from left to right. In each row following, we shift that sequence and determine the number of bits that are "the same" in the sequence.

Consider that the $\boldsymbol{D_A}$ input sequence could be coming from a transmitter and the receiver is attempting to synchronize by comparing shifted versions of the known sequence. We see that only one shift relationship matches "perfectly." All other shifted patterns show three matches. Reassure yourself that complementing the original pattern by changing all "1" to "0" and "0" to "1" would make the matches 0 of 7 in row number seven and 4 of 7 elsewhere. We expect any random sequence of seven bits to have 3 or 4 matches most often and a "perfect" match or mismatch seldom if ever. We use this property to determine synchronization boundaries for the PRBS sequence in normal or complemented form.

For every "bit" of QPSK data, we will substitute one complete sequence of seven bits from the PRBS. We will use the sequence whenever the QPSK is to represent a "1" and complement the sequence whenever a "0" is to be represented.

Table 7.2 PRBS Sequence (Right) Autocorrelation

D_A	1	1	0	1	0	0	0	
Shift								**Matches**
1	0	1	1	0	1	0	0	3
2	0	0	1	1	0	1	0	3
3	0	0	0	1	1	0	1	3
4	1	0	0	0	1	1	0	3
5	0	1	0	0	0	1	1	3
6	1	0	1	0	0	0	1	3
7	1	1	0	1	0	0	0	7

In Table 7.2 above, we show similar autocorrelation results with the second rightmost sequence we have presented in Table 7.0 above.

Table 7.2 PRBS Sequence Crosscorrelaton

D_A	1	0	1	1	0	0	0	
Shift								**Matches**
1	**0**	**1**	**1**	**0**	**1**	**0**	**0**	**3**
2	**0**	**0**	**1**	**1**	**0**	**1**	**0**	**5**
3	**0**	**0**	**0**	**1**	**1**	**0**	**1**	**3**
4	**1**	**0**	**0**	**0**	**1**	**1**	**0**	**3**
5	**0**	**1**	**0**	**0**	**0**	**1**	**1**	**1**
6	**1**	**0**	**1**	**0**	**0**	**0**	**1**	**5**
7	**1**	**1**	**0**	**1**	**0**	**0**	**0**	**5**

In Table 7.2 above, we show the $\boldsymbol{D_A}$ input sequence from the first sequence, but in each row following, we shift the $\boldsymbol{D_A}$ input sequence from our second sequence and determine the number of bits that are "the same" in the sequence.

Consider that the $\boldsymbol{D_A}$ input sequence could be coming from a transmitter and the receiver is attempting to synchronize by comparing shifted versions of the known sequence, but does not yet know which pattern is in which channel. We see that no shift relationship matches "perfectly."

Reassure yourself that complementing the original pattern by changing all "1" to "0" and "0" to "1" would never make a perfect match. We expect any random sequence of seven bits to have 3 or 4 matches most often and a "perfect" match or mismatch seldom if ever. We use this property to determine synchronization boundaries for the PRBS sequence for channel identification.

Clearly identifiable auto-correlation and cross-correlation properties make the recovery of the sequence synchronization and channel identification possible, if not easy, in DSSS systems.

Further, for both PRBS sequences, the quantity of "1" and "0" symbols in the sequence is as close to equal as is possible with an odd number of bits. This property ensures that the upper and lower sidebands will contain nearly equal energy contributions from the data. Any DC components of both QPSK ***I*** and **Q** data streams are ameliorated by the spreading using the PRBS.

As another note, in a run length of seven bits, each code generated has only one occurrence of any sequence of the same number of equal bits. The distribution of run-lengths is similar to a property of a random sequence, but limited by the finite length of the sequence. It is this

run-length property that lends the “Pseudo-Noise” (PN) description to the PRBS signals. The PN property tends to spread the energy of the spectrum evenly as we sill see in later illustrations

We have chosen PN sequences for spreading, but for other services there are other sequences with good auto-correlation and cross-correlation properties, notably the Walsh functions widely used in Code-Division, Multiple-Access (CDMA) applications but we have chosen the simple sequences for pedagogy.

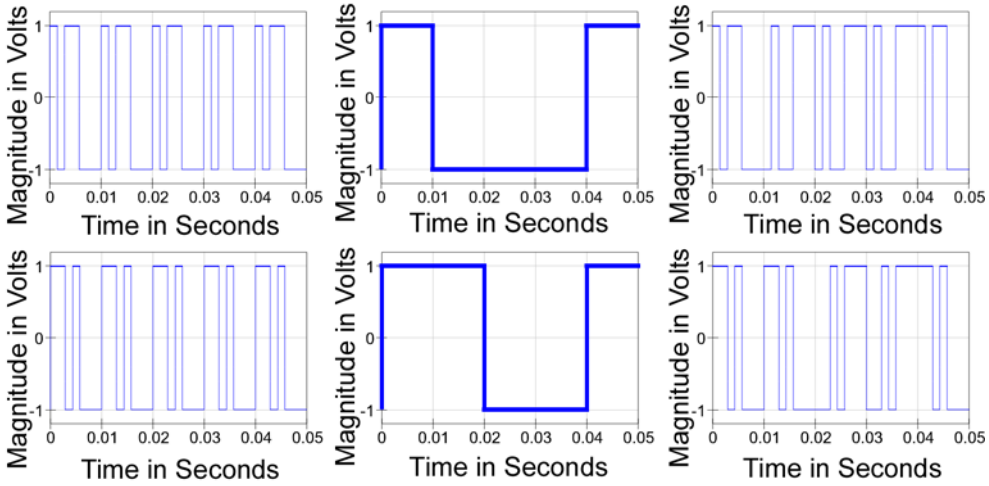

Figure 7.1 The Two PN Examples with Original Data Streams and Spread Result

In figure 7.1 above, we show the two distinct PN example sequences with a sequence length adjusted to be equal to 10 msec, the length of the data sequence bits in each channel. We also show the spread result of a multiplication of the PN sequence by the data sequence and the complement of the PN sequence at each negative value of the data. Notice that the upper sequence is complemented at the 10 msec instant and returns to the non-complemented version again at the 40 msec instant. The lower sequence is complemented at the 20 msec instant and returns to the non-complemented version again at the 40 msec instant. With this sequence run length of seven, and the subsequent multiplication, the digital data is increased by 7X to 700 bits per second from the original 100 bits per second.

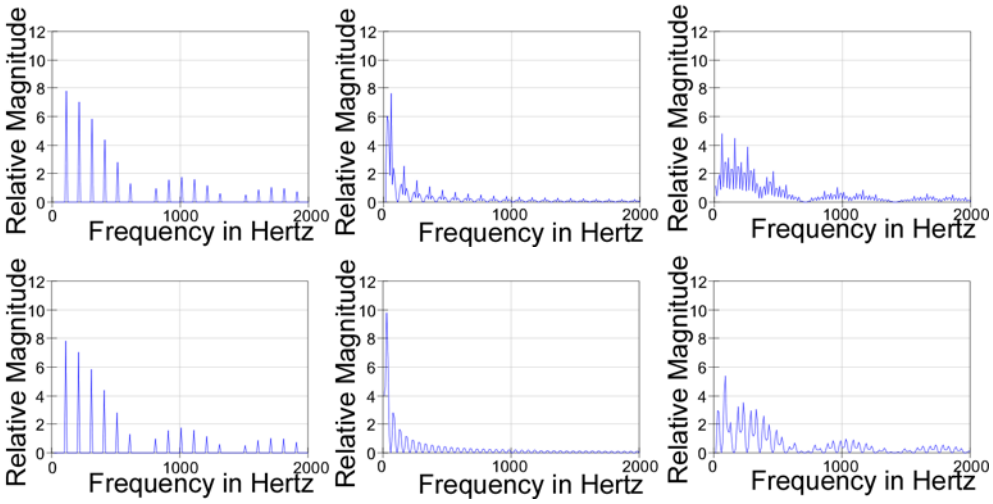

Figure 7.2 The Two PN Spectra, Original Data Spectra and Spread Spectra

In figure 7.2 above, we show the same two distinct PN example sequences, but in the frequency domain. The PN Sequences exhibit distinct spectral lines with no appreciable DC component. The original data shows spectral with a fundamental AC component that is much lower than the PN sequences, as well as a DC component. The spread spectrum for each channel shows a much more complex spectrum with spectral nulls that match the PN sequence as a consequence of the PN having no energy at those frequencies. In addition, there is essentially no DC component, and implies that we can expect truly suppressed carrier behavior when we later use the two spread sequences to be the ***I*** and the ***Q*** information to QPSK modulate the carrier frequency.

In figure 7.3 below, we show the same two distinct PN example sequences used in a correlator to de-spread the ***I*** and the ***Q*** sequences. The correlation shown is an exclusive-OR of the spread sequence with the original PN sequence and does not involve modulation onto the carrier. It is used to show that the correlation retrieves the original sequence. The subsequent lowpass filtering of the correlated data shows “ringing” artifacts of the lowpass filter used to remove correlator “glitches” and is implementation specific. The same filter is employed to illustrate later the behavior of cross-correlation and mis-timed correlation de-spreading.

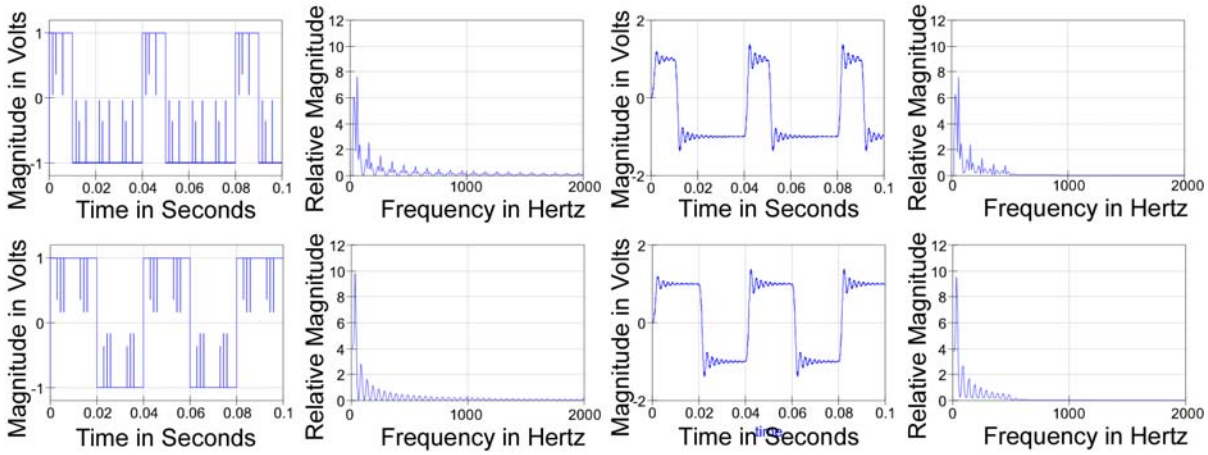

Figure 7.3 Correct Correlations and Spectra, With Filtered Waveforms and Spectra

In figure 7.3 above, we show that the original data can be recovered from the spread spectrum by correlating the spread sequence with the originating PN sequence. In figure 7.4 below, we show the result of cross-correlation with the opposite PN sequence resulting in no recognizable data sequence.

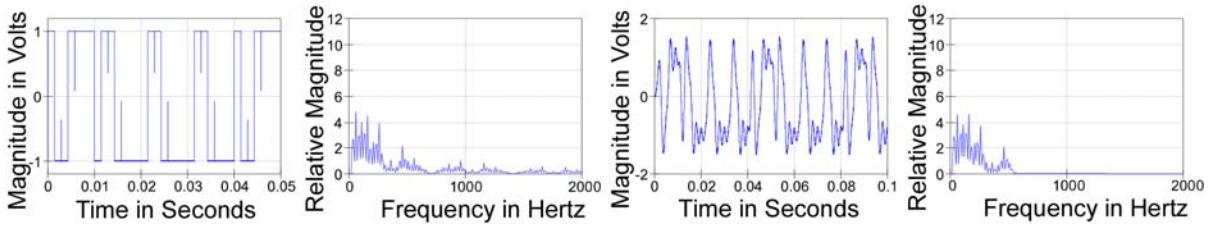

Figure 7.4 Cross Correlations and Spectra, With Filtered Waveforms and Spectra

In figure 7.4 above, we show that cross-correlation of the sequence that is spread with one PN sequence is not de-spread using the other PN sequence but results in a waveform with little or no 100 bits per second data. The consequence of this behavior is an assurance that only the correct PN sequence can be used to recover data from the spread spectrum sequence and that same behavior permits the resolution of which channel contains the ***I*** channel's information and which contains the ***Q*** channel's information because each is associated with its own unique PN sequence.

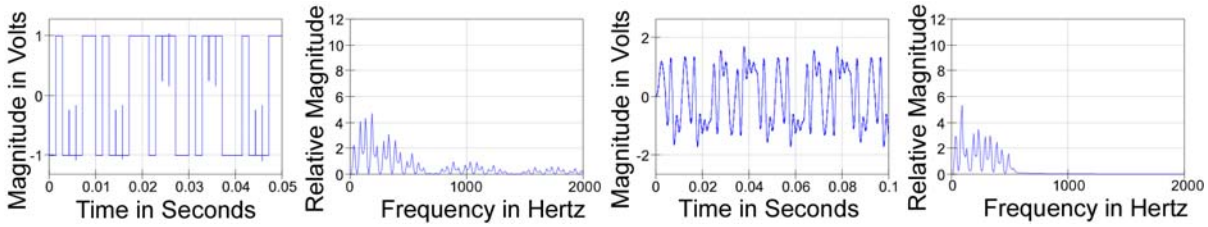

Figure 7.5 Delayed Correlations and Spectra, With Filtered Waveforms and Spectra

In figure 7.5 above, we show that auto-correlation of the sequence that is spread with the correct PN sequence, but a delayed version of the PN sequence for data de-spreading is similar to using an incorrect sequence. The consequence of this behavior is the ability to use delayed versions of each PN sequence in a de-spreading correlation series to determine the correct sequence synchronization. Because the de-spreading correlation only occurs with a match of PN sequences as well as PN sequence delays, the de-spreading correlation provides a timing signal consequent with correct sequence auto-correlation that is synchronous with the original data transition clocking and hence provides a recovered data clock.

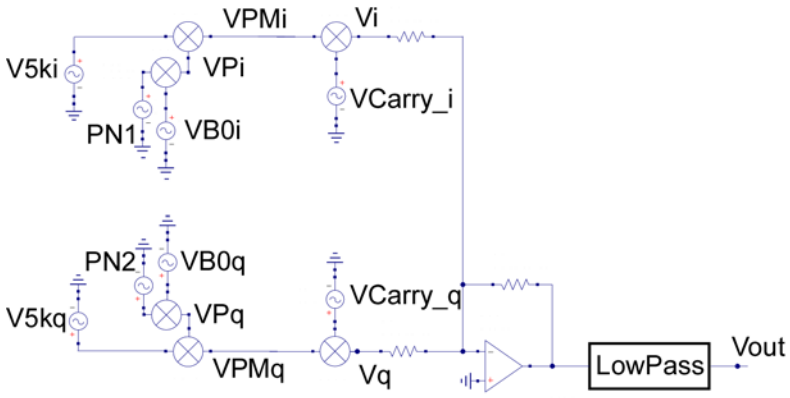

Figure 7.6 Weaver Modulator for Spread-Spectrum QPSK

In prior discussions we have developed the modified Weaver architecture in the context of QPSK, and in figure 7.6 above, we add the spreading ***PN1*** and ***PN2*** components to produce the "new" ***VPi*** (top) and ***VPq*** (bottom) phase modulating multiplier inputs. We now refer to the raw 100 bits per second data sequence sources by the ***VB0i*** and ***VB0q*** designators. Figure 7.1 and 7.2 above show the development of the sequences and spectra of the signals that compose the ***VPi*** and ***VPq*** phase modulating multiplier inputs.

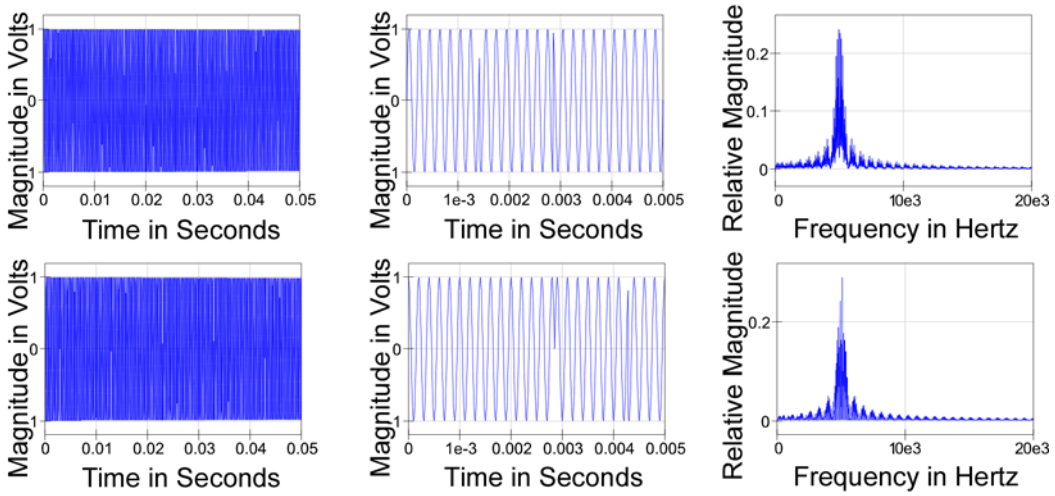

Figure 7.7 *VPMi* (top) and *VPMq* (bottom), Details, and Spectra

In figure 7.7 above, we see the result of employing the spread spectrum sequences to modulate the 5 kHertz quadrature reference tones. The ***VPMi*** and ***VPMq*** result is a constant magnitude signal with 180^{o} phase reversals at each edge of the ***VPi*** and ***VPq*** phase modulating sequences. The spectrum is much wider than the QPSK spectrum shown in the previous figure 6.3 above. Despite the binary nature of the modulation, the relatively low data rate produces sine wave segments for multi-millisecond intervals.

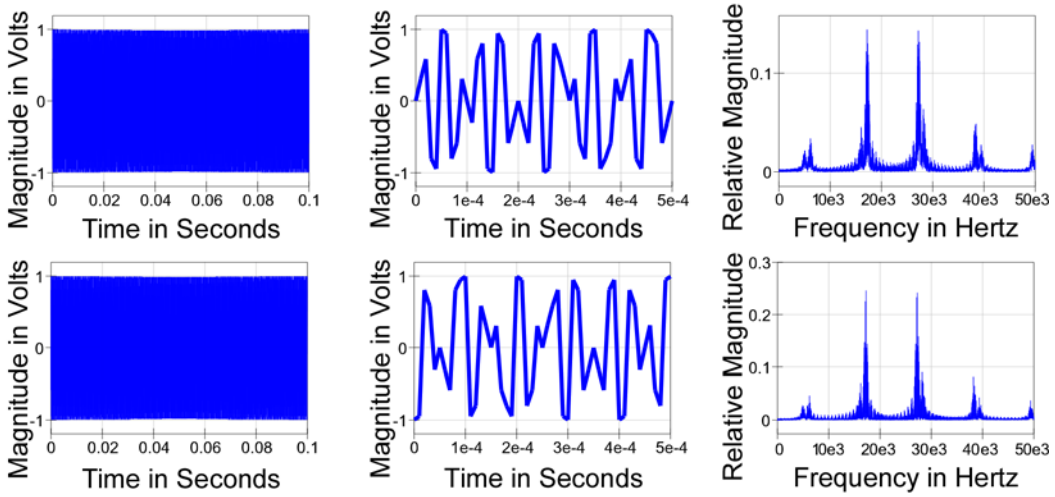

Figure 7.8 *Vi* (top) and *Vq* (bottom), *Vi* (top) and *Vq* (bottom) Detail, and Spectra

In figure 7.8 above, we see the result of employing the 22 kHertz quadrature carrier frequency square wave sources to modulate the ***VPMi*** and ***VPMq*** signals. The 22 kHertz

carrier frequency is much higher than the spread spectrum modulated tone frequency and the result reveals ***Vi*** and ***Vq*** signals with pronounced "choppy" sine wave segments. These results, at the sub-millisecond time scale are nearly indistinguishable in the time domain from the QPSK results shown in figure 6.4 above, with the notable exception of the much wider spectrum occupied around the sum and difference frequencies when spreading is applied. Likewise, the square wave harmonics are present and require filtering for removal. Further, both the sum and difference signals for both ***Vi*** and ***Vq*** signals are nearly the same peak spectral magnitude in the sideband pairs with essentially no 22 kHertz carrier remnants.

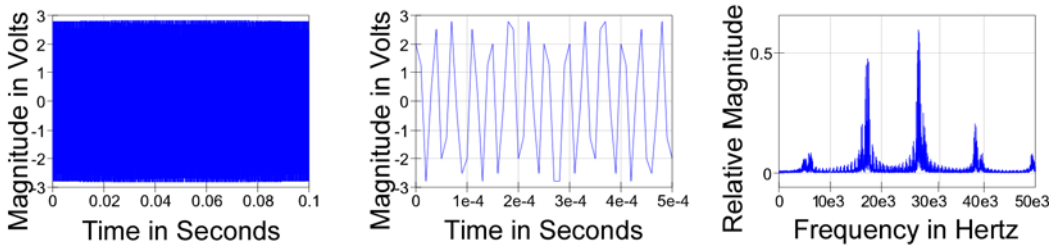

Figure 7.9 Un-Filtered Sum of *Vi* and *Vq* Signals Detail, and Spectrum

In figure 7.9 above, we show the un-filtered sum of the ***Vi*** and ***Vq*** signals with notably different spectral peak magnitudes in the upper and lower sidebands 5 kHertz on either side of the 22 kHertz suppressed carrier.

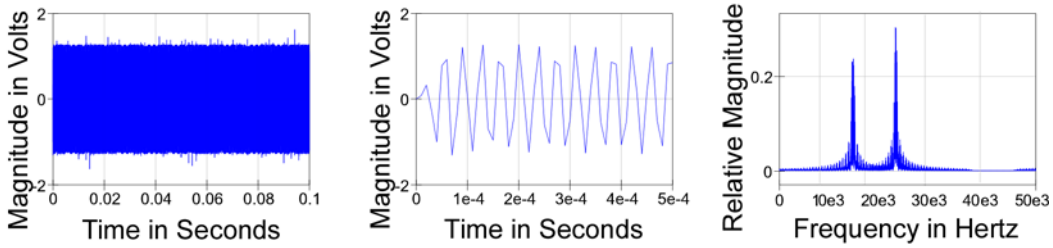

Figure 7.10 *Vout* Low Pass Filtered Sum of *Vi* and *Vq* Signals Detail, and Spectrum

In figure 7.10 above, we show the filtered sum of the ***Vi*** and ***Vq*** signals with notably "cleaner" energy spectral peaks in the upper and lower sidebands, but still no significant 22 kHertz carrier or DC signal. This signal is representative of a double-sideband, suppressed carrier signal with a spread spectrum QPSK sub-carrier at 5 kHertz..

8.0 DSSS – Sub-Carrier Demodulation

Again, we employ the Weaver modulator to introduce the demodulation processes for signal recovery. The architecture is identical to that shown in figure 6.7, but is repeated locally as figure 8.0 below.

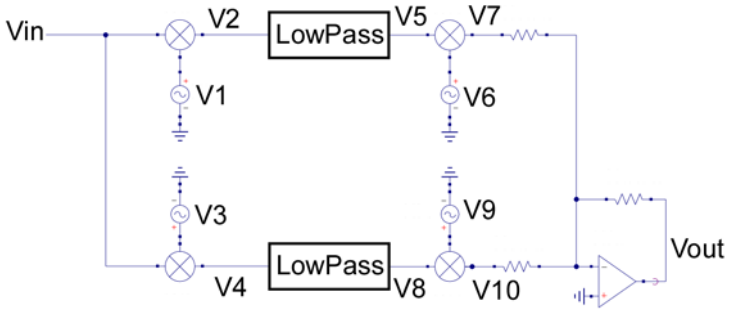

Figure 8.0 Weaver Modulator Used for Demodulation Discussion

In figure 8.0 above, we show the Weaver structure used for demodulation of the ***Vout*** signal shown in figure 7.10 above. The demodulation structure is used only in this local context for discussion of demodulation issues. At the location of the quadrature source pair ***V1*** and ***V3*** in figure 8.0 above, we employ a replica of the ***VCarry_i*** and ***VCarry_q*** square wave quadrature signal pair for demodulation and connect the ***Vin*** input terminal to the filtered ***Vout*** signal shown in figure 7.10 above. For this discussion, we defer how to obtain the ***V1*** and ***V3*** quadrature pair with synchronism to the ***VCarry_i*** and ***VCarry_q*** square waves.

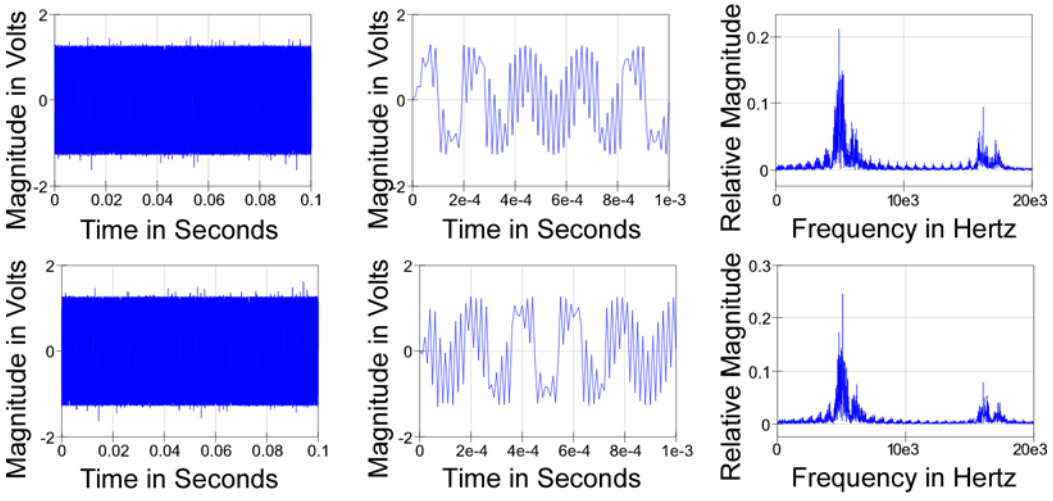

Figure 8.1 *V2* (top) and *V4* (bottom), *V2* (top) and *V4* (bottom) Detail, and Spectra

In figure 8.1 above, we show the waveforms of the ***V2*** (top) and ***V3*** (bottom) signals developed in the de-modulator of figure 8.0 above. We see a constant envelope, phase modulation signals, but in the detail we see remnants of the square wave nature of the ***V1*** (used in the top) and ***V3*** (used for the bottom) signals used as the carrier quadrature demodulation pair because the detail phase changes from the multiplication are abrupt. The ***V2*** (top) and ***V4*** (bottom) spectra produced have harmonic multiples of the 22 kHertz carrier square waves (not shown here), along with the modulation spectra around them, and now show the difference frequency components produced at the 5 kHertz demodulation frequency.

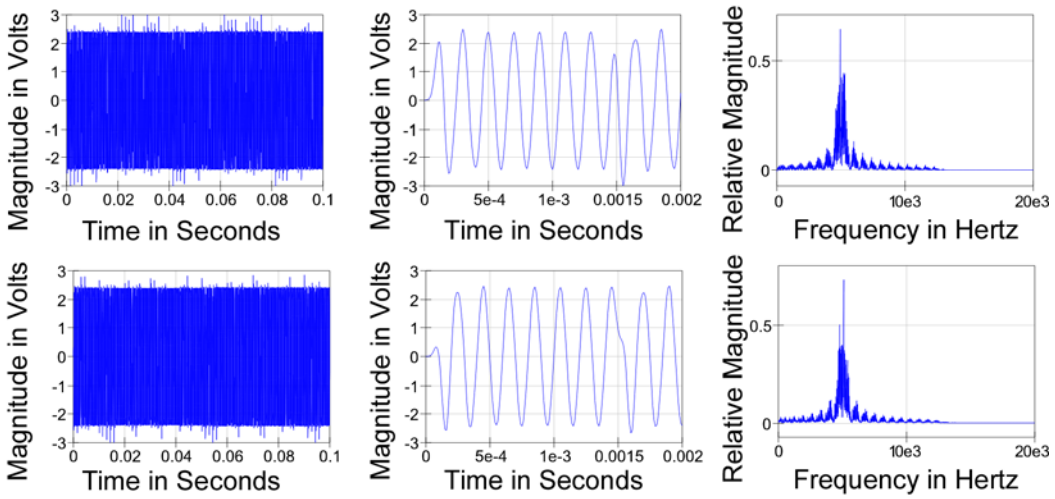

Figure 8.2 *V5* (top) and *V8* (bottom), *V5* (top) and *V8* (bottom) Detail, and Spectra

Filtering the ***V2*** (top) and ***V4*** (bottom) signals leaves the ***V5*** (top) and ***V8*** (bottom) filtered signals that replicate the ***VPMi*** and ***VPMq*** phase-modulated signals produced in the prior figure 7.7 of the transmitting Weaver modulator. These signals are spread-spectrum QPSK replicas, but there are well-known issues of identifying which replica channel represents which transmitter channel, as well as the exact frequency/phase synchronization of the ***V1*** and ***V3*** signals with the ***VCarry_i*** and ***VCarry_q*** square wave quadrature signal pair used in the transmitter. We defer that discussion until after we have introduced the pseudo-noise correlation of the QPSK transmitted signal and discussed its synchronization in a receiver.

9.0 DSSS: Minimum Structure Direct Sequence Modulation

The discussion has employed the QPSK spread-spectrum modulation of the 5 kHertz sub-carrier in the Weaver modulator architecture. We now dispense with the sub-carrier and perform direct modulation at the carrier frequency. The sidebands are no longer as distinct as

in the prior case, but the implementation is simpler and differences are explored. The sub-carrier approach is used in multiple access with multiple sub-carrier frequencies and "sequencies" of orthonormal digital functions for some applications, but the following discussion is most commonly labeled as "direct-sequence" modulation.

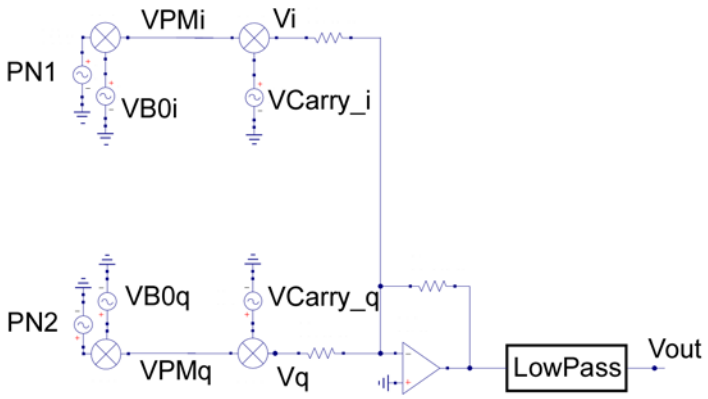

Figure 9.0 Modulator for Direct Sequence Spread-Spectrum QPSK

In figure 9.0 above, we see that the spread sequences ***VPMi*** and ***VPMq*** are applied directly as the phase modulation data for the ***VCarry_i*** and ***VCarry_q*** square wave quadrature signal pair used in the transmitter. We see in figure 8.1 below, that we will not have distinguishable sideband pairs with upper and lower sidebands distinct, but we shall see that they still exist, just much closer to the carrier frequency. The spectra appear to have energy at 22 kHertz.

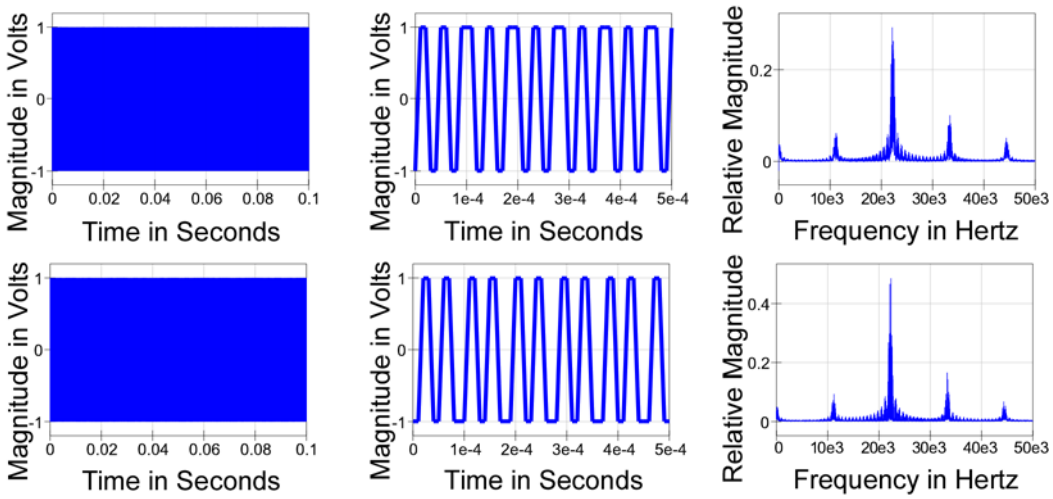

Figure 9.1 *Vi* (top) and *Vq* (bottom), *Vi* (top) and *Vq* (bottom) Detail, and Spectra

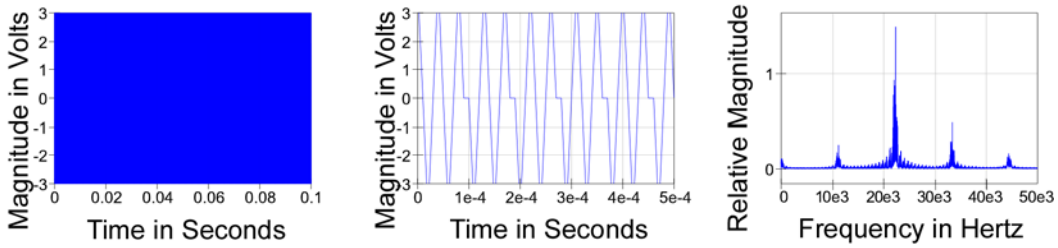

Figure 9.2 Un-Filtered Sum of *Vi* and *Vq* Signals Detail, and Spectrum

In figure 9.2 above, we show the un-filtered sum of the ***Vi*** and ***Vq*** signals with no notably different spectral characteristics either side of the 22 kHertz suppressed carrier.

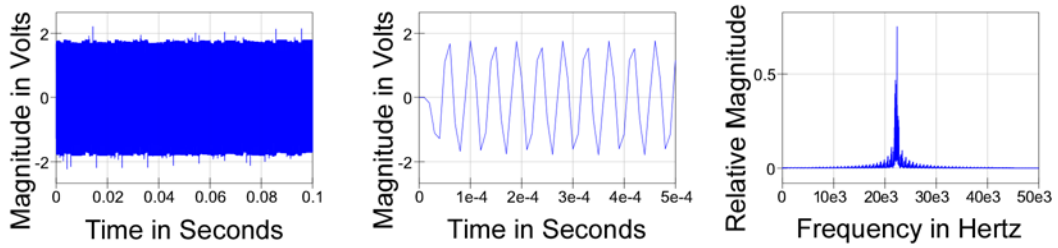

Figure 9.3 *Vout* Low Pass Filtered Sum of *Vi* and *Vq* Signals Detail, and Spectrum

In figure 9.3 above, we show the filtered sum of the ***Vi*** and ***Vq*** signals with a notably "cleaner" energy spectrum. In figure 9.4 below, we see the narrow-band spectrum near the 22.22 kHertz (the more precise carrier frequency), and the double-sideband, suppressed carrier nature is more readily apparent.

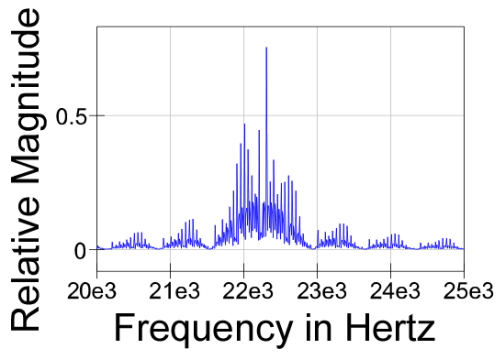

Figure 9.4 *Vout* Spectrum Detail

10.0 DSSS – Direct Sequence Demodulation

As before, we utilize the Weaver modulator for received signal discussions, as shown in figure 8.5 below.

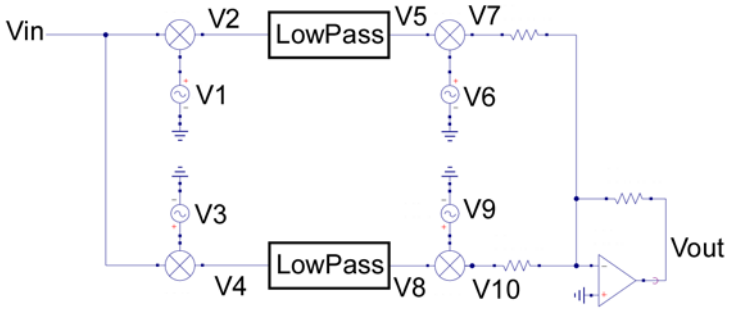

Figure 10.0 Weaver Modulator Used for Demodulation Discussion

In figure 10.0 above, we show the Weaver structure used for demodulation of the ***Vout*** signal shown in figure 9.4 above. The demodulation structure is used only in this local context for discussion of demodulation issues. At the location of the quadrature source pair ***V1*** and ***V3*** in figure 10.0 above, we employ exact replicas of the ***VCarry_i*** and ***VCarry_q*** square wave quadrature signal pair for demodulation and connect the ***Vin*** input terminal to the filtered ***Vout*** signal shown in figure 7.10 above. For this discussion, we defer how to obtain the ***V1*** and ***V3*** quadrature pair with synchronism to the ***VCarry_i*** and ***VCarry_q*** square waves, but we stress the importance of synchronous reconstruction in the results.

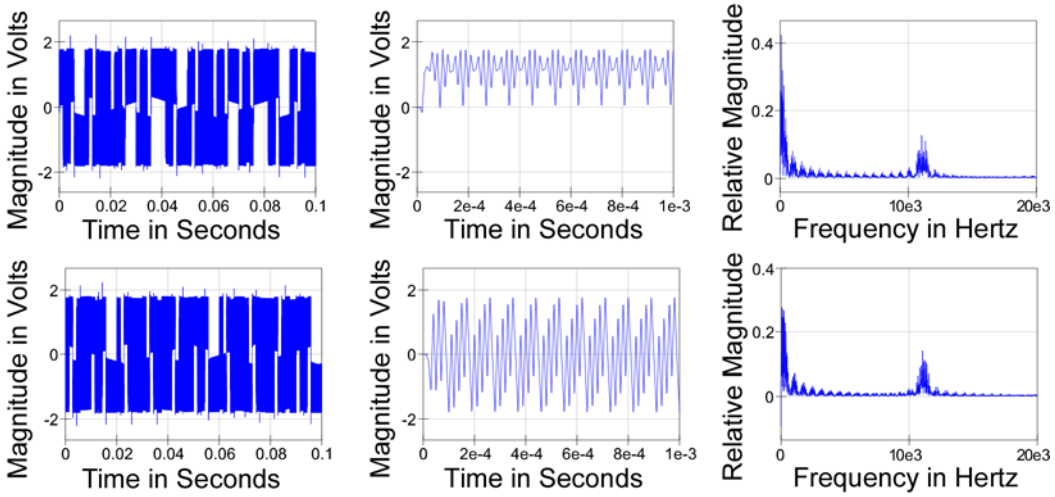

Figure 10.1 *V2* (top) and *V4* (bottom), *V2* (top) and *V4* (bottom) Detail, and Spectra

In figure 10.1 above, we show the waveforms of the ***V2*** (top) and ***V3*** (bottom) signals developed in the de-modulator of figure 10.0 above. We see a constant envelope, phase modulation signals, but in the detail we see unrecognizable reconstructions of ***VPMi*** and ***VPMq*** signals used as the carrier quadrature modulation pair. The ***V2*** and ***V4*** spectra produced do not seem unreasonable, but we shall see in figure 10.2 below that we have lost all recognition of the original of ***VPMi*** and ***VPMq*** signals used in the process of employing exact replicas ***VCarry_i*** and ***VCarry_q*** C

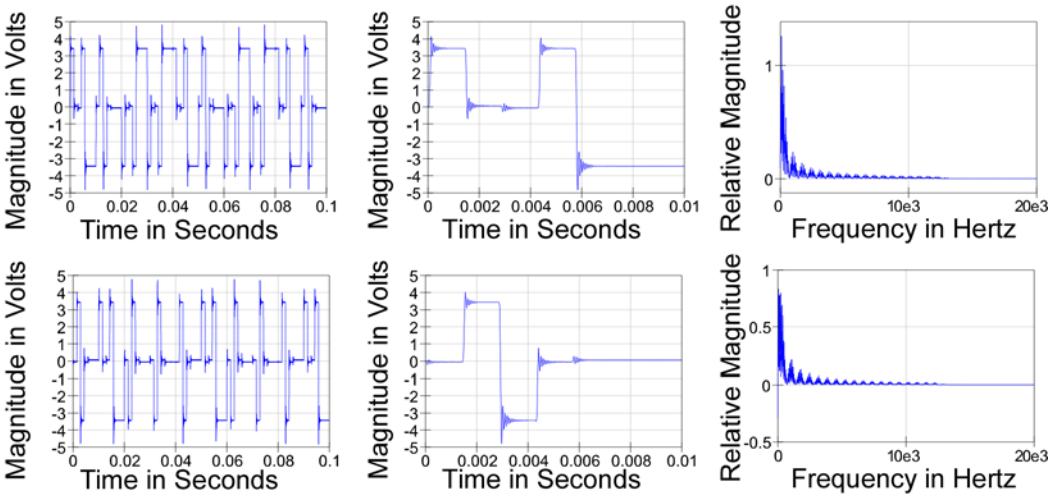

Figure 10.2 *V5* (top) and *V8* (bottom), *V5* (top) and *V8* (bottom) Detail, and Spectra

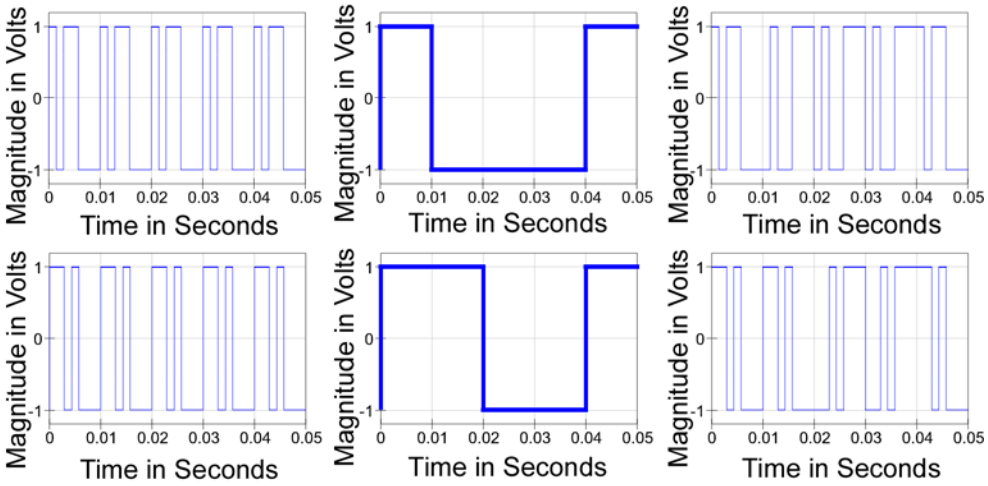

Figure 10.3 The Two PN Examples with Original Data Streams and Spread Result

For reference, we reproduce in figure 10.3 above, the PN sequences, the original data stream, and the spread result that we have employed as the ***VPMi*** and ***VPMq*** signals in the transmitting modulator. We expected the ***V5*** and ***V8*** signals to be replicas of the ***VPMi*** and ***VPMq*** signals.

We observe, however, that the ***V5*** and ***V8*** signals are not replicas of the ***VPMi*** and ***VPMq*** signals, but rather show distinct intermediate levels with a recovered value of "0" instead of the "+1" or "-1" expected. We attribute the "cancellation" as indication that some of the ***I*** information is present in the ***Q*** channel, and visa versa. This is a clear indication that the quadrature source pair ***V1*** and ***V3*** are incorrect replicas of the ***VCarry_i*** and ***VCarry_q*** square wave quadrature signals, at least in terms of their phase relationships.

In our example, the "culprit" is the delay associated with the transmitter's low pass filter used to remove the harmonics from the ***Vout*** signal. For a receiver at a location remote from the transmitter, the situation is similar but far worse. In our example, we have prior knowledge of the exact frequency and phase of the ***VCarry_i*** and ***VCarry_q*** square wave quadrature signals, but that information in the general case is not available and must be reconstructed. The suppressed carrier nature of the signal ensures that there is intentionally no energy available at the requisite frequency. Once we do have the correct carrier phase reconstruction, however, the recovered data appears as in figure 10.4 below.

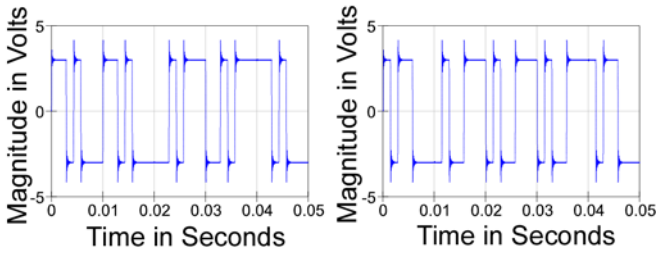

Figure 10.4 *V5* and *V8*, with Synchronized *V1* and *V3* Quadrature Pair

11.0 DSSS – Carrier recovery

The suppressed carrier communication presents issues in obtaining the exact frequency/phase synchronization of the ***V1*** and ***V3*** signals with the ***VCarry_i*** and ***VCarry_q*** square wave quadrature signal pair used in the transmitter. There are two methodologies employed in practical systems for carrier recovery, a squaring loop and the Costas loop. There are

mathematical derivations that prove they are equivalent in performance, but there are substantial implementation issues.

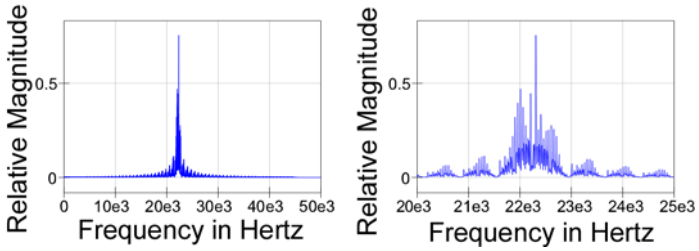

Figure 11.0 Wide-Band *Vout* Spectrum, and Narrow-Band Spectrum Detail

We know that the spectrum of the Vout signal is located around the 22 kHertz carrier frequency, and that there is substantially no energy at that carrier frequency, nor any harmonics transmitted that we can employ for synchronization.

We show below that we can develop such a signal from the channel signal itself by mixing the channel signal with itself in a square-law manner. Adding signals A plus B and squaring the sum follows the simple identity:

$$(A+B)^2 = A^2 + 2AB + B^2 \qquad [11.1]$$

The upper and lower sideband signals from the prior ***Vout*** summation are the A and B quantities as follows:

$$A+B = V_i \cos\left(2\pi F_{Carry} t + \phi PM_i\right) + V_q \sin\left(2\pi F_{Carry} t + \phi PM_q\right) \qquad [11.2]$$

We produce sum and difference terms from the AB product, as well as DC terms and twice frequency terms. We see below in figure 11.1 that the algebraic square has produced energy at 44 kHertz. In the narrow-band spectrum, we see a distinct spectral line at 44.44 kHertz, and a narrow-band filter shows that the energy at that second harmonic can be obtained from the result. Amplification and limiting can produce a “square-wave” at the second harmonic. A digital frequency divider pair, one with transitions on the second harmonic rising edge, and the other with transitions on the second harmonic falling edge, produces a quadrature pair in synchrony with the energy in the double-sideband, suppressed carrier signal.

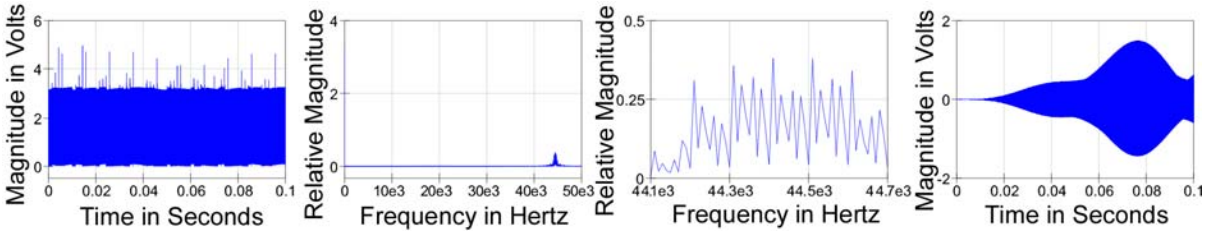

Figure 11.0 Wide-Band *Vout* Spectrum, and Narrow-Band Spectrum Detail

The famous Costas loop achieves the same squaring result but utilizes phase-lock loop techniques in its implementation and permits receiver reference locking at 90^{o} intervals. Detail implementation of a Costas loop will not be included here or discussed, but some mechanism for carrier reconstruction and synchronism is required.

12.0 DSSS: I & Q PN synchronization

We have chosen PN sequences with good auto-correlation and reasonable cross-correlation behavior, knowing that identification of the sequence can resolve the identification of which is the ***I*** channel information and consequent ***Q*** channel information by the correlation behaviors. First, however, the transitions of the PN sequences must be identified and synchronized to a "chip" or sequence clocking/spreading rate. For the two PN sequences we have used in our example, each complete cycle of the PN sequence is seven bits in duration and at a rate 7X the data rate of 100 bits per second. Therefore, to correctly establish the boundaries between data bits, we must first establish the "chip" clock at 7X that rate.

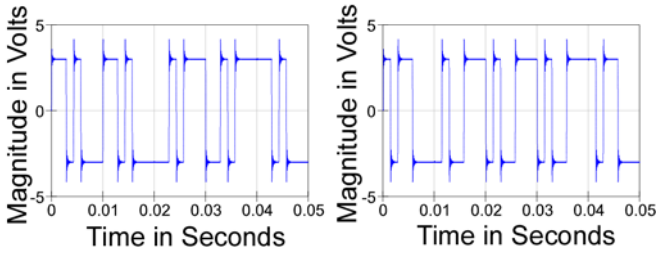

Figure 12.0 *V5* and *V8*, with Synchronized *V1* and *V3* Quadrature Pair

The polarity of the received ***V5*** and ***V8*** signals is modulated 180^{o} at the edges of the PN "chip" sequence times by the binary data. Consequently, we do not know which polarity is expected, but we do know that each edge must occur with timing at a rate 7X greater than the expected data rate. Because the PN chip polarity is only important following synchronization, we first synchronize using the edges of the PN "chip" patterns as follows below.

In figure12.1 below, we see the received ***I*** and ***Q*** patterns on the ***V5*** and ***V8*** signals. We amplify the signals with a clipping amplifier and obtain the edge timing signals from each transition of either polarity.

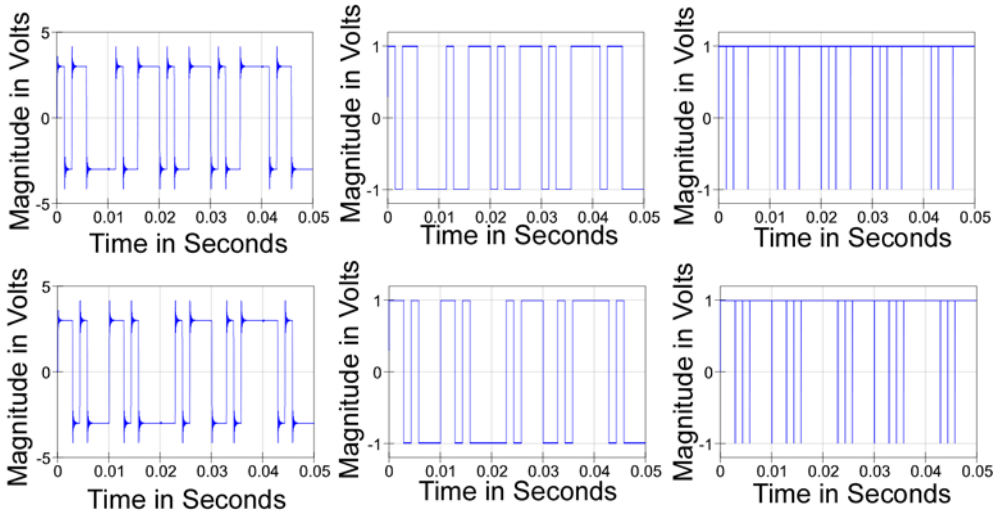

Figure 12.1 *V5* and *V8*, Saturated signals, and Edge Timing Signals

With a high signal to noise ratio, synchronizing the timing using edges is effective, but the better approach is to employ the "matched filter" or correlator shown in figure 12.2 below.

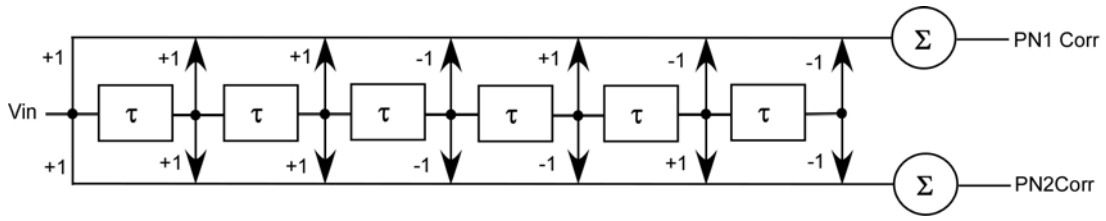

Figure 12.2 *V5* or *V8* is Vin and PN1 Corr and PN2 Corr are Filter Outputs

In figure12.2 above, we see a series of delay blocks with the delay **τ** constructed as the expected "chip" clock delay. The delay is asynchronous, but as close to the expected clock period as possible. At each delay stage, we sum the signals with a weight given by the PN sequence in reverse order. The first bit of the PN sequence experiences the greatest delay (six clock periods), and the last PN sequence bit experiences no delay. The S block adds the contributions from each PN sequence bit, scaled by its expected polarity according to the +1, or –1 weight. In this manner, the sequence is the "dot-product" of the sequence received with the PN sequence generator weights. The same delay series is used for both summations

because we have no prior knowledge of the carrier synchronization phase and its polarity contribution. In figure 12.3 below, we see the signals present at each stage of the delay series for one of the received sequences.

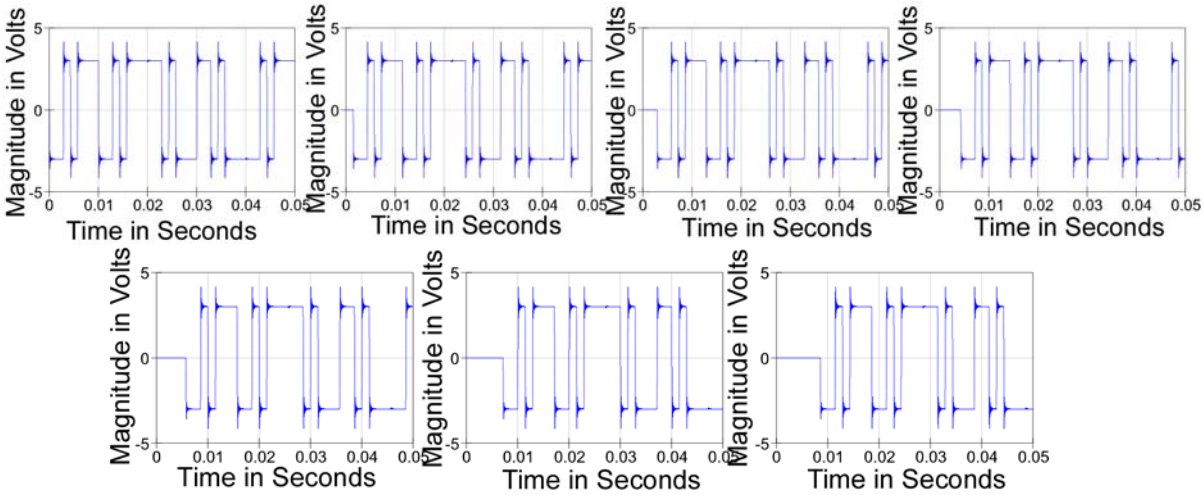

Figure 12.3 One Received Channel Signal Plus and Each Delay Stage Signal

In figure12.3 above, we see the series of delayed replicas of the channel signal. With those signals combined we obtain a pair of PN Corr signals for the ***I*** channel and another pair for the ***Q*** channel as shown in figure 12.4 below. Once we have gone to the trouble of constructing the delayed replicas, we obtain two PN correlation patterns from one structure.

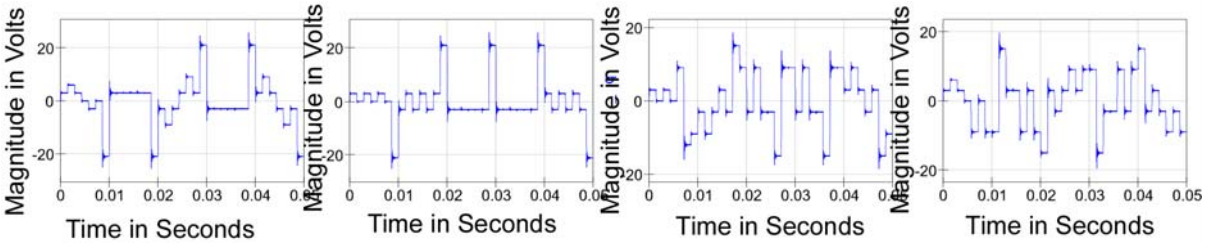

Figure 12.4 Correlator Output Signals

In figure12.4 above, we have shown the first two signals with the "correct" PN sequence behavior indicating that the ***Vin*** signal to the correlator "matches" the code weight pattern of the structure. The remaining two output signals are the simultaneous result of a signal fron the PN sequence that does not match the code weight pattern of the structure. Each structure has its input from either the ***V5*** or ***V8*** signal, so we know it can only match one or the other.

In figure12.4 above, in the first two panels, we see that the "matched filter" has summed the PN sequence energy from all seven bits to a peak in each PN sequence once per "chip" cycle

pattern. That correlation identifies the end of the "chip" boundary, as well as the polarity of the data bit during that prior chip period. Further, the summation of the energy over the prior entire "chip" period into the last bit of the chip period is key to the effectiveness of PN sequence spreading. In figure 12.3, we see that each bit provides a peak signal magnitude of approximately Volts, but the Correlator provides 7 times that signal level during the last bit period.

$$V_{Correlator} = \sum_{i=1}^{7} W_i \bullet V_{Delay\_i} \qquad [12.0]$$

As we can see from equation [12.0], the maximum correlation occurs with a coherent match of the signal with the weights and any other signal sequence has a reduced output. Further, any Additive White Gaussian Noise (AWGN) present with the signal is averaged over the seven cycles, but the coherent signal adds constructively and improves the Signal-to-Noise Ratio (SNR) during the last bit of the "chip" period. SNR improvement is possible with longer chip sequences, but processing delay also increases.

In figure 12.4 above, we see that the maximum magnitude signals from each correlator occurs with the "chip" periodicity and permit identification of the chip synchronism, as well as the data bit clock synchronism. Because the correlator is an asynchronous structure, at least at the PN sequence clocking rate, it is not necessary to explicitly recover the PN sequence clock, but some applications may require such a signal for the construction of a reply channel, without the need for a precise internal clock.

13.0 Pseudo-Noise: I & Q Bit Stream Recovery

The Correlator structure permits a bit stream decision at the maximum correlation bit in the "chip" sequence. That maximum correlation bit timing, for our example, corresponds in both the ***I*** and ***Q*** channels, further enhancing the decision process. Unfortunately, the uncertainty involved in the carrier synchronization requires coding in the data bit sequence to resolve polarity issues.

The data stream can be encoded using a "Manchester" code with data polarity signified by the presence or absence of data transitions ate particular timing intervals, Another candidate for a channel code is a "delay-modulated code" that also offers higher data rates by finer resolution of transition timing. Each code offers particular advantages but can resolve the issue of polarity uncertainty.

14.0 Code Division Multiple Access (CDMA)

We have employed PN sequences only for spreading, but there also exist "orthonormal" digital sequences with good autocorrelation and cross-correlation properties. With one common platform, but a change of code, multiple communication links can co-exist in the same bandwidth. This variation of DSSS is known as "Code-Division. Multiple Access" communication, and is widely used in cell-phone services.

The cross-correlation of codes causes the signal from one code to appear similar to a "noise" because the lack of coherence prevents the summation of equation [12.0] from being constructive. The energy of an interfering signal is not eliminated, but it is reduced in effect due to its lack of coherence. The auto-correlation properties make Walsh functions poor candidates fro spectrum spreading, however.

Combinations of codes may be used for spreading a signal for different purposes. In the CDMA 2000 code spreading, for example, A Walsh transform, a "Long" code constructed from a 42 bit shift-register, and a "Short" code constructed from a 15 bit shift-register are all used. CDMA 2000 uses 256 Walsh sequences to provide 64 channels, the "Short" code for PN spreading, and the "Long" code for encryption and authentication.

Table 14.0 Walsh Functions (0) through (16)

Sequence Number	Bit Number 1	2	3	4	5	6	7	8	9	10	11	12	13	14	15	16
1	1	1	1	1	1	1	1	1	0	0	0	0	0	0	0	0
2	1	1	1	1	0	0	0	0	0	0	0	0	1	1	1	1
3	1	1	1	1	0	0	0	0	1	1	1	1	0	0	0	0
4	1	1	0	0	0	0	1	1	1	1	0	0	0	0	1	1
5	1	1	0	0	0	0	1	1	0	0	1	1	0	0	1	1
6	1	1	0	0	1	1	0	0	0	0	1	1	0	0	1	1
7	1	1	0	0	1	1	0	0	1	1	0	0	1	1	0	0
8	1	0	0	1	1	0	0	1	1	0	0	1	1	0	0	1
9	1	0	0	1	1	0	0	1	0	1	1	0	0	1	1	0
10	1	0	0	1	0	1	1	0	0	1	1	0	1	0	0	1
11	1	0	0	1	0	1	1	0	1	0	0	1	0	1	1	0
12	1	0	1	0	0	1	0	1	1	0	1	0	0	1	0	1
13	1	0	1	0	0	1	0	1	0	1	1	0	1	0	1	0
14	1	0	1	0	1	0	1	0	0	1	0	1	0	1	0	1
15	1	0	1	0	1	0	1	0	1	0	1	0	1	0	1	0

In Table 14.0 above, we reproduce the 15 of the 16 Walsh functions. Walsh Function (0) is a DC level and does not show correlation with any of the other functions, but is equivalent to

an un-coded channel. Spreading the data with a Walsh function provides multiple channels in the same spectrum and is performed first in the transmitting process and last in the receiving process. The Walsh functions do not have good auto-correlation properties and are used after synchronism is achieved by the "short" code or PN sequence.
Because Walsh functions are "orthonormal," a group of data streams can be combined by binary addition without any carry bits and still be retrieved by an inverse operation at a receiver. It is the combined data stream that is PN spread by the "Short" code and the entire bit sequence is available simultaneously at each end of a conversation. In CDMA cell-phone services, only the "base station" uses all channels at once.

Many variations of coding are available, and services use added levels of coding for security and access control.

15.0 Summary and Conclusions

This course has developed the theory and some practical issues using a consistent example case leading up to Direct Sequence Spread Spectrum (DSSS) Communication. The information theoretic foundation of trading bandwidth for improved Signal-to-Noise Ratio (SNR) was introduced mathematically, but other useful properties associated with the particular spreading sequence properties used in the example were introduced later. The gradual development based on the Weaver architecture for frequency translation of single-sideband, suppressed carrier signals through digital QPSK examples into pseudo-noise (PN) sequence spreading of QPSK of sub-carrier sidebands and finally to direct-sequence, spread-spectrum QPSK was employed and built awareness of the relationships between the spectral energy and the modulation processes in both the time and frequency domains.

The PN sequence generation, its auto-correlation and cross-correlation attributes were introduced and employed in the example with a justification for the development of the matched-filter/correlator approach to sequence de-spreading. Some issues of carrier synchronization and problems were introduced but not developed in detail. Finally, the statistical properties of the correlator approach were shown to be the basis for Code-Division, Multiple Access (CDMA) spectrum sharing to ameliorate somewhat the extra bandwidth occupied by the spreading.

